



**International
Collaboration
Center**

Institute for Materials Research
Tohoku University

ICC-IMR FY2017 Activity Report

<http://www.icc-imr.imr.tohoku.ac.jp/>

ICC-IMR FY2017

Activity Report

International Collaboration Center

Institute for Materials Research
Tohoku University

CONTENTS



Mission	02
Committee Members	03
Visiting Scholars	05
Integrated Projects	18
Workshops	24
KINKEN WAKATE	30
Short-term Visiting Researchers	33
Young Researcher Fellowships	45



Mission

The ICC-IMR was founded in April 2008 as the center for international collaboration of the Institute for Materials Research (IMR) a center of excellence in material science, consisting of 27 research groups and five research centers. The ICC-IMR works as a gateway of diverse collaborations between overseas and IMR researchers. The ICC-IMR has invited 53 visiting professors and conducted 20 international research projects since its start-up (please inspect the graph below for more details,). The applications are open to foreign researchers and the projects are evaluated by a peer-review process involving international reviewers.

ICC-IMR coordinates six different programs:

- 1) International Integrated Project Research
- 2) Visiting Professorships
- 3) Short Single Research Visits
- 4) International Workshops
- 5) Fellowship for Young Researcher and PhD Student
- 6) Material Transfer Program

We welcome applicants from around the globe to submit proposals!

Visitors supported by ICC-Programs.



ICC-IMR COMMITTEE MEMBERS

Director

Prof. Gerrit E. W. BAUER

Steering Committee

Prof. Eiji SAITOH

Prof. Hiroyuki NOJIRI

Prof. Hitoshi MIYASAKA

Prof. Shin-ichi ORIMO

Prof. Akira YOSHIKAWA

Prof. Hidemi KATO

Prof. Masaki FUJITA

Activity Report

Visiting Scholars



FY 2017 Visiting Scholars

No.	Candidate	Host	Proposed Research	Title	Affiliation	Term
17G01	Yongmin Kim	Prof. Nojiri	Transport and Tunneling Properties of 2D Van der Waals Heterostructures	Professor	Dankook University, Korea	2017.5.1-7.31
17G02	Weerapong Chewpraditkul	Prof. Yoshikawa	Luminescence and Scintillation Properties of $(\text{Lu}_x\text{Gd}_{3-x})(\text{Al}_{2.4}\text{Ga}_{2.6})\text{O}_{12}:\text{Ce}$, $x = 0.2, 0.4, 0.6, 0.8$ Multicomponent Garnet Crystals	Associate Professor	King Mongkut's University of Technology Thonburi, Thailand	2017.6.5-7.8
17G03	Jianfeng Zhang	Prof. Goto	Precipitation of SiC on Superhard Diamond Particles and its Spark Plasma Sintering Combined with WC	Professor	Hohai University, China	2017.10.1-12.31
17G04	Zlatko Sitar	Prof. Matsuoka	The Metalorganic Vapor Phase Epitaxial Growth of InGaAlN	Professor	North Carolina State University	2018.1.9-3.31

Optical and transport properties of semiconductor nanostructures and 2D van der Waals heterostructures under high magnetic fields

Guest Professor: Yongmin Kim Dankook University, Korea

Host Professor: H. Nojiri, IMR

We proposed to study optical properties of semiconductor quantum structures, transport and tunneling properties of two-dimensional layered materials during my guest faculty period at the IMR. We obtained significant optical transitions from MAPbX₃ (X=Cl, Br, I) under high magnetic fields. Unlike the optical measurements, we failed to observe transport and tunneling characteristics from graphene multilayers. This may be due to the aging effect of the sample.

My term as a guest professor at the IMR – Tohoku University was May 1 2017 to July 31, 2017. The host professor was Prof. H. Nojiri. During that period, we try to investigate the optical properties of semiconductor nanostructures, and the transport and tunneling properties of two-dimensional (2D) layered materials under high magnetic fields. We did obtain anomalous photoluminescence (PL) transitions from methyl-ammonium lead halide (MAPbX₃ (X=Cl, Br, I)), which is known as hybrid organic inorganic perovskite crystals. MAPbX₃ families are known to be used as next generation solar cells and LEDs. Therefore, tremendous research reports are under coming last few years. We obtained peculiar optical transitions from a MAPbI₃ crystal under high magnetic fields, which is a square root B dependency of peak transition energy. This is due may to the variation of the effective g factor in the presence of magnetic field. The conduction band structure in such perovskite materials has SOC band, which is the band minimum at the R point. A strong spin-orbit interaction can change effective g factor in magnetic fields. Consequently, the square root B dependency of the transition energy can possibly be occurred due to the strong spin-orbit interaction in the conduction band.

The material used for this study receives tremendous attention all over the world due to its potential application on the photovoltaic devices. The efficiency of the solar cell device by using this material already approaches to the silicon based solar cell devices, which was achieved only within last five years. There are numerous unknown carrier dynamics occurred in this material. The magneto-optical investigations on this material can be a valuable work to

find such unknown carrier dynamics in this materials, which will guide to increase the solar efficiency for future photovoltaic device applications.

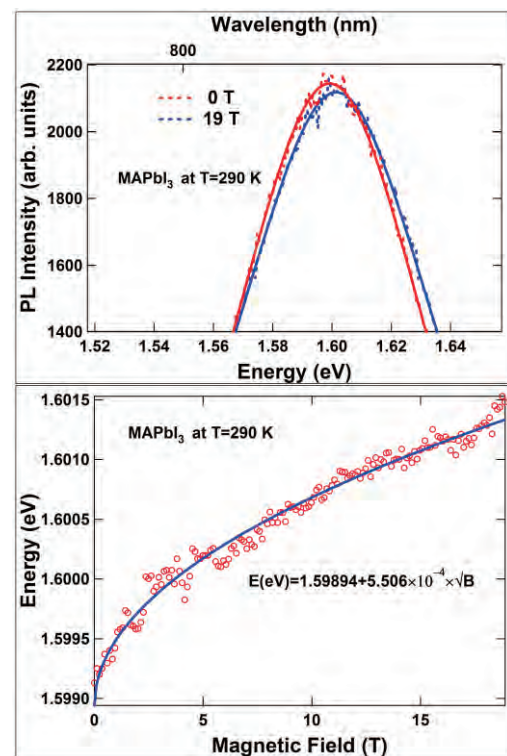


Fig.1 (upper) PL spectra at 0 and 19 T. The peak at 19 T shows blue shift. (lower) Peak transition energy vs magnetic field. Circles and solid line indicate experimental and fitted data, respectively. The experimental data follows a square root B fitting curve.

We tried to investigate tunneling properties of Au-h-BN-Graphene structure under magnetic fields. Figure 2 inset shows the

schematic diagram of the sample used for this study.

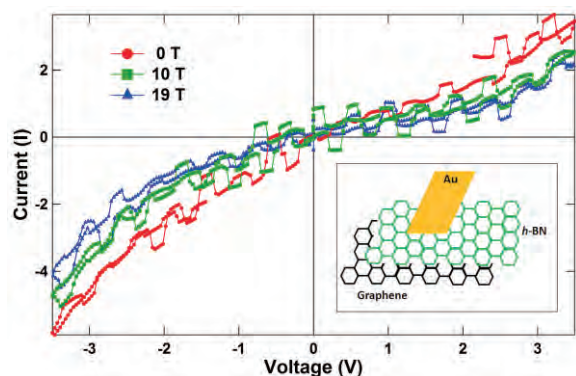


Fig. 2 I-V characteristics of Au - *h*-BN - Graphene tunnel structure (inset). Red, green and blue colors are I-V curves at 0, 10 and 19 T.

As seen in Fig. 2, red, green and blue markers are the I-V curves under magnetic fields at 0, 10 and 19 T, respectively. In this figure, we do not clearly distinguish I-V curves between 0 and 10 T. There is small change at 19 T. We realized that the sample can be contaminated by oxygen, water and/or O-H when it is exposed to the air, which can deteriorate the I-V characteristics. The sample used for this study was exposed at least a month in the air. Therefore, the I-V characteristics in this study cannot be reliable. We planned to redo the experiments with fresh samples.

In summary, we have measured optical transitions of MAPbX_3 ($X=\text{Cl, Br and I}$) hybrid organic-inorganic perovskite crystals and magneto-tunneling properties of an Au-*h*-BN-graphene tunnel device. We obtained anomalous optical transition from a MAPbI_3 single crystal under high magnetic fields. This is due may to the strong spin-orbit coupling, which modifies the effective g factor of the conduction and electrons in the presence of magnetic field. For tunneling properties of Au-*h*-BN-graphene device, due to the contamination by the air exposure for a long time, the device characteristics are vague. We planned to

Keywords : hybrid organic-inorganic perovskite, tunnel device, magneto-optical transition (spin-orbit coupling, effective g factor)

Full Name: Yongmin Kim (Department of Physics, Dankook University, Korea)

E-mail: yongmin@dankook.ac.kr

<http://www.dankook.ac.kr/en/web/international>

Luminescence and scintillation properties of (Lu_xGd_{3-x})(Al_{2.4}Ga_{2.6})O₁₂:Ce multicomponent garnet crystals

Assoc. Prof. Weerapong Chewpraditkul

(King Mongkut's University of Technology Thonburi, Bangkok 10140, Thailand)

This report summarizes my research work during five-week visit as a Visiting Associate Professor at Yoshikawa's Laboratory, Institute of Materials Research (IMR), Tohoku University, from June 5 to July 8, 2017.

The purpose of the visit was to investigate the scintillation properties of new multicomponent garnet crystals (Lu_xGd_{3-x})(Al_{2.4}Ga_{2.6})O₁₂; doped with Ce and codoped with Ce + Mg. These crystals were grown by micro-pulling down method.

1. Crystal growth and characterization

LuGdAGG:Ce and LuGdAGG:Ce,Mg crystals were grown by the micro-pulling-down method using an RF heating system (Fig.1). Starting materials with the composition (Lu_xGd_{3-0.015-x})(Al_{2.4}Ga_{2.6})O₁₂:Ce_{0.015} and (Lu_xGd_{3-0.0165-x})(Al_{2.4}Ga_{2.6})O₁₂:Ce_{0.015}Mg_{0.0015}, $x = 0.2, 0.4, 0.6, 0.8$ were prepared by mixing of 99.99% pure oxide materials at a stoichiometric composition. An Ir crucible was used in the atmosphere of Ar + 2%O₂ to prevent evaporation of gallium oxide. The seed was undoped GAGG crystal rod attached to the alumina seed holder (Fig. 2). The pulling rate was 0.05 mm/min and the crystal diameter was around 4 mm. The photograph of as grown (Lu_{0.6}Gd)AGG:Ce0.5% crystals is shown in Fig. 3. The polished plates of about 3.8 x 3.8 x 2 mm cut from the parent rods were used for all the measurements, i.e. X-ray induced RL spectra, scintillation decay time and light yield value.

The RL spectra measurements were performed using CCD- coupled monochromator under excitation with X-ray tube (20 kV, 0.15 mA). Fig.4 shows the RL spectra of the μ -PD grown (Lu_{0.8}Gd)AGG:Ce and (Lu_{0.8}Gd)AGG:Ce,Mg crystal samples compared to the CZ-grown GAGG:Ce crystal. The blue-shifted of RL spectra for the studied crystals with respect to the



Fig.1. Photograph of the μ -PD growth machine.

GAGG:Ce crystal was clearly observed. It can be attributed to the decrease in the crystal field strength around Ce³⁺ ion at the dodecahedral site from a partial substitution of Gd³⁺ by the smaller Lu³⁺ ions, which causes a high-energy shift of the 5d₁ level of Ce³⁺ center.



Fig.2. An Ir crucible attached to the after-heater and GAGG seed mounted to the alumina rod.

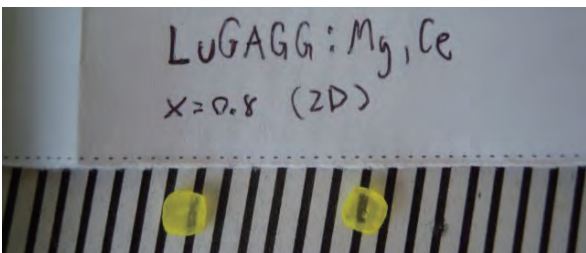
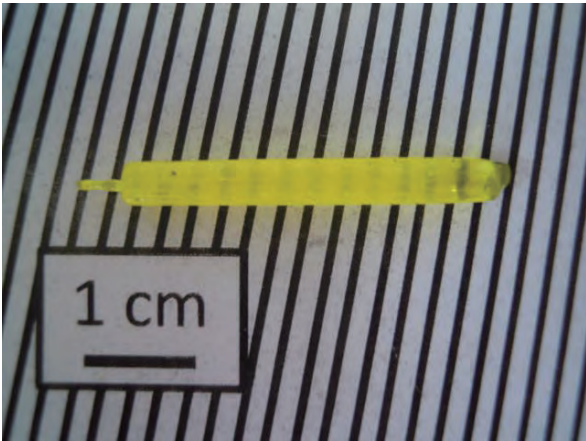


Fig.3. Photograph of $(\text{Lu}_{0.6}\text{Gd})\text{AGG}:\text{Ce}$ crystals grown by the $\mu\text{-PD}$ method.

The scintillation decay time measurements were performed using a Hamamatsu R7600U-200 PMT and Tektronix TDS3052 digital storage oscilloscope under excitation with γ - rays from a ^{137}Cs source. Fig.5 presents examples of the scintillation decay spectra of $(\text{Lu}_x\text{Gd})\text{AGG}:\text{Ce}$ crystals in comparison with Mg^{2+} -codoped $(\text{Lu}_x\text{Gd})\text{AGG}:\text{Ce},\text{Mg}$ crystals.

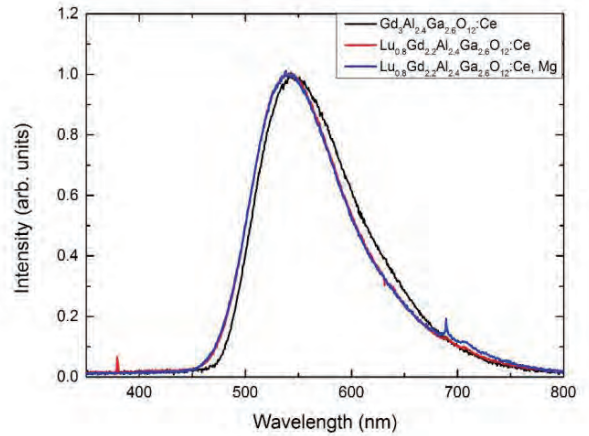


Fig.4. RL spectra of $\mu\text{-PD}$ grown $(\text{Lu}_{0.8}\text{Gd})\text{AGG}:\text{Ce}$ and $(\text{Lu}_{0.8}\text{Gd})\text{AGG}:\text{Ce},\text{Mg}$ samples compared to the CZ-grown GAGG:Ce crystal.

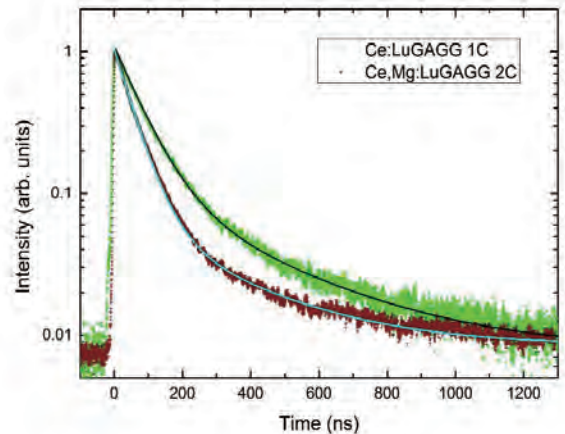
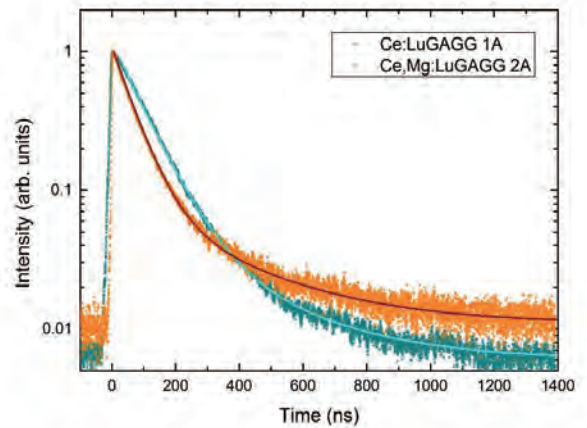


Fig.5. Scintillation decays of some $\mu\text{-PD}$ grown $(\text{Lu}_x\text{Gd})\text{AGG}:\text{Ce}$ and $(\text{Lu}_x\text{Gd})\text{AGG}:\text{Ce},\text{Mg}$ crystals.

The decay time components and relative intensities were estimated using a double-exponential fit to the scintillation decay spectra, and the results are collected in Table 1. The Mg co-doped crystals show a faster decay time with respect to LuGdAGG:Ce crystals.

Table.1. Scintillation decay time and relative intensity of the $(\text{Lu}_x\text{Gd})\text{AGG}:\text{Ce}$ and $(\text{Lu}_x\text{Gd})\text{AGG}:\text{Ce},\text{Mg}$ crystals.

Crystals	$\tau_1(\text{I}\%)$ ns	$\tau_2(\text{I}\%)$ ns
(1A) Lu _{0.2} GAGG:Ce	85(83%)	290(17%)
(1B) Lu _{0.4} GAGG:Ce	72(76%)	340(23%)
(1C) Lu _{0.6} GAGG:Ce	72(65%)	318(35%)
(1D) Lu _{0.8} GAGG:Ce	68(73%)	290(27%)
(2A) Lu _{0.2} GAGG:Ce, Mg	62(72%)	296(28%)
(2B) Lu _{0.4} GAGG:Ce, Mg	56(71%)	280(29%)
(2C) Lu _{0.6} GAGG:Ce, Mg	52(74%)	280(26%)
(2D) Lu _{0.8} GAGG:Ce, Mg	52(73%)	266(27%)

Light yield (LY) measurements were performed using a Hamamatsu R6231 PMT under excitation with a ^{137}Cs γ - rays. To improve the light collection efficiency each sample was coupled to the PMT window with silicone grease and covered with several layers of Teflon tape. The signal from the PMT anode was processed by a CANBERRA 2005 preamplifier and a Tennelec TC243 spectroscopy amplifier set at 4 μs shaping time constant. Tukan 8 k MCA was used to record the pulse height spectra. The photoelectron yield (phe/MeV) was determined by relating the full-energy peak position with that of the single photoelectron peak from the PMT photocathode. Fig. 6 shows the pulse height spectra of ^{137}Cs γ - rays measured with the μ -PD grown $(\text{Lu}_{0.2}\text{Gd})\text{AGG}:\text{Ce}$ and $(\text{Lu}_{0.2}\text{Gd})\text{AGG}:\text{Ce},\text{Mg}$ crystals compared to the old $\text{Gd}_3\text{Al}_2\text{Ga}_3\text{O}_{12}:\text{Ce}$ (GAGG:Ce) CZ-grown crystal. The LY (ph/MeV) was calculated using the PMT average quantum efficiency of 13% for the emission spectrum of both crystals. The best crystal sample (Lu_{0.2}GAGG:Ce, Mg) shows very good pulse height spectrum of 662 keV γ - rays from a ^{137}Cs source due to its good crystal quality. It exhibits LY value of 43,300 ph/MeV and energy resolution of 9.3% in comparison -

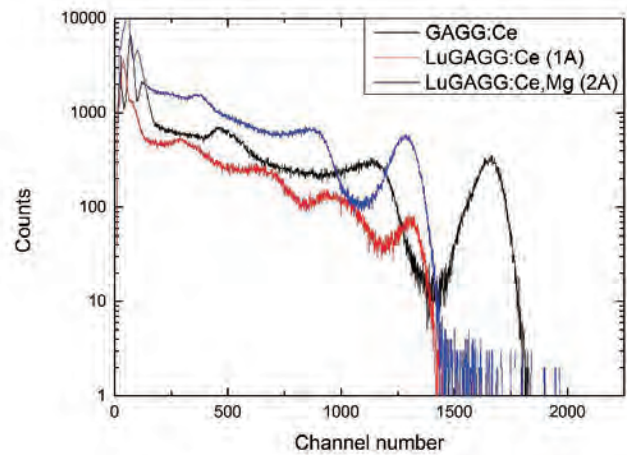


Fig.6. Pulse height spectra of ^{137}Cs gamma rays measured with the studied $(\text{Lu}_{0.2}\text{Gd})\text{AGG}:\text{Ce}$ and $(\text{Lu}_{0.2}\text{Gd})\text{AGG}:\text{Ce},\text{Mg}$ crystals compared to a CZ-grown $\text{Gd}_3\text{Al}_2\text{Ga}_3\text{O}_{12}:\text{Ce}$ crystal.

to the values of 56,100 ph/MeV and 6.9% for the old CZ-grown GAGG:Ce crystal.

2. Topics of Other Activities (Assistance to IMR Staff, Students, etc.)

Characterizing the scintillation properties of Mg^{2+} - and Li^{1+} - codoped GAGG:Ce crystals

$\text{Gd}_3(\text{Al}_{2.4}\text{Ga}_{2.6})\text{O}_{12}:\text{Ce},\text{Mg}$ and $\text{Gd}_3(\text{Al}_{2.4}\text{Ga}_{2.6})\text{O}_{12}:\text{Ce},\text{Li}$ crystals (with dimension $5\times 5\times 5\text{ mm}^3$) were grown by the Czochralski method and the scintillation characteristics were investigated and compared to the old CZ-grown GAGG:Ce crystal. Fig. 7 shows pulse height spectra of 662 keV γ - rays from a ^{137}Cs source measured for the studied crystals with same size of $5\times 5\times 5\text{ mm}^3$. LY and energy resolution are collected in Table 2. The LY value of 46,326 ph/MeV measured for the $\text{Gd}_3(\text{Al}_{2.4}\text{Ga}_{2.6})\text{O}_{12}:\text{Ce},\text{Li}$ samples is larger than that of 44,768 ph/MeV for the old GAGG:Ce sample, whereas the $\text{Gd}_3(\text{Al}_{2.4}\text{Ga}_{2.6})\text{O}_{12}:\text{Ce},\text{Mg}$ samples show a lower LY value of 22,069 MeV and 27,027 MeV. Superior energy resolution of $\text{Gd}_3(\text{Al}_{2.4}\text{Ga}_{2.6})\text{O}_{12}:\text{Ce},\text{Li}$ crystals was also confirmed in the better LY-proportionality (see Fig. 8) in addition to a larger LY value.

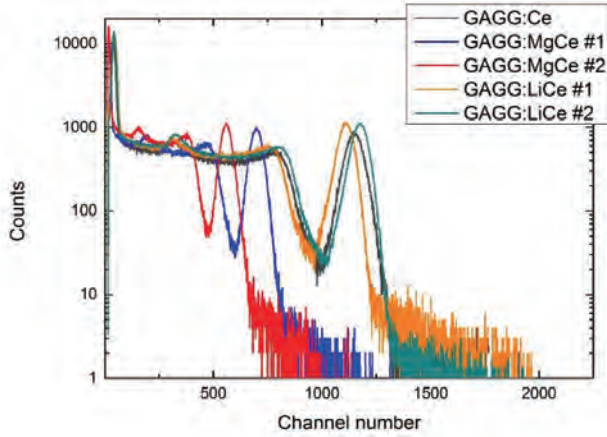


Fig.7. Pulse height spectra of 662 keV γ - rays from a ^{137}Cs source measured with $\text{Gd}_3(\text{Al}_{2.4}\text{Ga}_{2.6})\text{O}_{12}:\text{Ce},\text{Mg}$, $\text{Gd}_3(\text{Al}_{2.4}\text{Ga}_{2.6})\text{O}_{12}:\text{Ce},\text{Li}$ and GAGG:Ce crystals.

Table. 2 Light yield and energy resolution of studied crystals.

Sample	LY (ph/MeV)	$\Delta E/E(\%)$
GAGG:MgCe #1	27,070	9.4
GAGG:MgCe #2	22,070	10.8
GAGG:LiCe #1	43,810	6.9
GAGG:LiCe #2	46,330	7.0
GAGG:Ce (old)	44,770	8.6

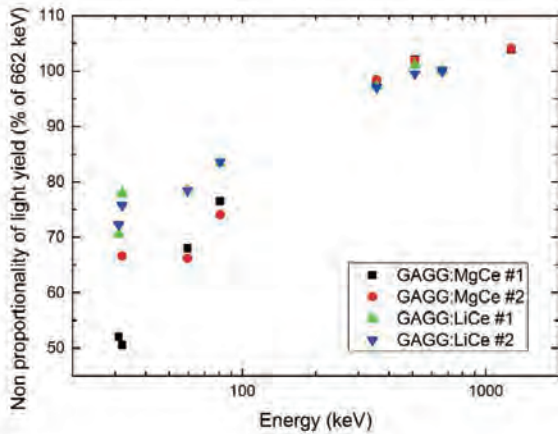


Fig. 8 LY non-proportionality of the studied crystals.

In order to investigate the scintillation timing characteristics, their scintillation decay spectra were measured as shown in Fig. 9. The decay time components (τ_i) were determined by performing a double exponential fit: $I(t) = \sum A_i \exp(-t/\tau_i) + B$. The results are collected in Table 5.

The $\text{Gd}_3(\text{Al}_{2.4}\text{Ga}_{2.6})\text{O}_{12}:\text{Ce},\text{Mg}$ crystals show faster scintillation decay time with respect to $\text{Gd}_3(\text{Al}_{2.4}\text{Ga}_{2.6})\text{O}_{12}:\text{Ce},\text{Li}$ and $\text{Gd}_3\text{Al}_2\text{Ga}_3\text{O}_{12}:\text{Ce}$. The coincidence time resolution for these crystals will be measured and discussed.

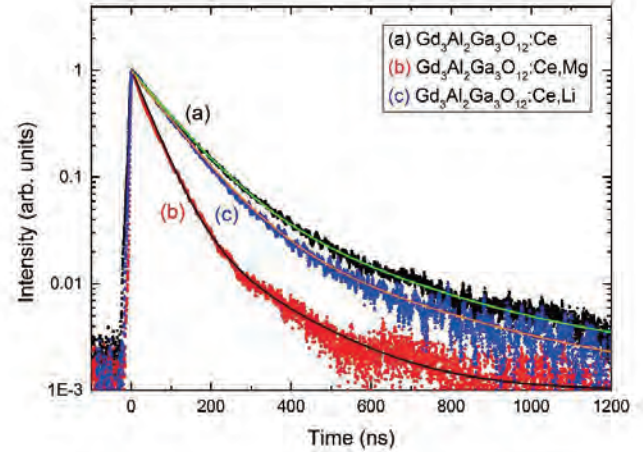


Fig. 9. Scintillation decay spectra of studied crystals

Table. 3. Scintillation decay of the studied crystals

Sample	$\tau_1(\text{ns})$ (I%)	$\tau_2(\text{ns})$ (I%)	$\tau_{\text{ave}}(\text{ns})$
GAGG:Ce	92 (76%)	300 (24%)	141
GAGG:Mg,Ce	46 (84%)	174 (16%)	66
GAGG:Li,Ce	90 (86%)	335 (14%)	124

3. Co-Authored Manuscript Preparation for Publication.

1. W.R. Chewpraditkul, N. Pattanaboonmee, W. Chewpraditkul, O. Sakthong, T. Szczesniak, M. Moszynski, K. Kamada, A. Yoshikawa, M. Nikl, Luminescence and scintillation characteristics of $(\text{Gd}_x\text{Y}_{3-x})\text{Al}_2\text{Ga}_3\text{O}_{12}:\text{Ce}$; $x = 1,2,3$ single crystals.
2. W.R. Chewpraditkul, N. Pattanaboonmee, O. Sakthong, W. Chewpraditkul, K. Kamada, A. Yoshikawa, M. Nikl, Scintillation properties of $\text{Gd}_3(\text{Al}_{5-x}\text{Ga}_x)\text{O}_{12}:\text{Ce}$; $x = 2.3, 2.6, 3.0$ single crystals.
3. O. Sakthong, W.R. Chewpraditkul, W. Chewpraditkul, T. Szczesniak, L. Swiderski, M. Moszynski, K. Kamada, A. Yoshikawa, M. Nikl, Comparative study of $\text{GdLu}_2\text{Al}_2\text{Ga}_3\text{O}_{12}:\text{Ce}$ and $\text{GdY}_2\text{Al}_2\text{Ga}_3\text{O}_{12}:\text{Ce}$ scintillation crystals for γ - ray detection.

4. Acknowledgments

I would like to thank all the members of Yoshikawa Laboratory and other Departments of IMR for their kind assistance and support.

July 2017

Keywords: Micro-pulling-down method; Scintillator;
Multicomponent garnet; Scintillation decays

E-mail: weerapong.che@kmutt.ac.th

Precipitation of SiC on superhard diamond particles and its spark plasma sintering combined with WC

As the hardest material, diamond has been used to enhance the hardness and fracture toughness of other cutting materials such as tungsten carbide or alumina. However, the using of Co sintering aid for WC would like to induce the phase transformation of diamond to graphite and lead to a volume expansion resulting in cracking and low hardness of the products. In the present study, SiC nanoparticles were precipitated on diamond by rotary MOCVD to increase the sinterability, and consequently improve the mechanical properties and reliability of diamond-based cutting tools.

Diamond has been widely used for cutting tools or as a reinforcing phase to enhance the hardness and wear resistance of other cutting materials, such as WC, Al₂O₃ and so on. However, these composites can hardly be densified by the traditional pressureless sintering or hot pressing because of the strong covalent bond and the easy phase transformation to graphite occurring at high temperatures, low pressure and long sintering time.

The recent literature indicates SiC is beneficial as a sintering aid for Diamond[1]. In the present study, the SiC nanolayer was precipitated on diamond powders by a rotary CVD apparatus[2, 3] using hexamethyldisilane (Si₂(HMDS) as a precursor. The HMDS precursor was heated to a vaporization temperature of 303 K and carried into the reactor by Ar gas at a flow rate of $1.7 \times 10^{-7} \text{ m}^3\text{s}^{-1}$, and the supply rate of precursor vapor was $6 \times 10^{-7} \text{ kgs}^{-1}$. The reactor chamber was rotated at 15 rpm with a total pressure in the reactor chamber at 400 Pa, the deposition temperature was 953 K, and the deposition time was varied from 10.8 to 14.4 ks. Fig. 1 shows that the SiC nanolayer was about 20-50 nm in thickness was successfully precipitated on Diamond.

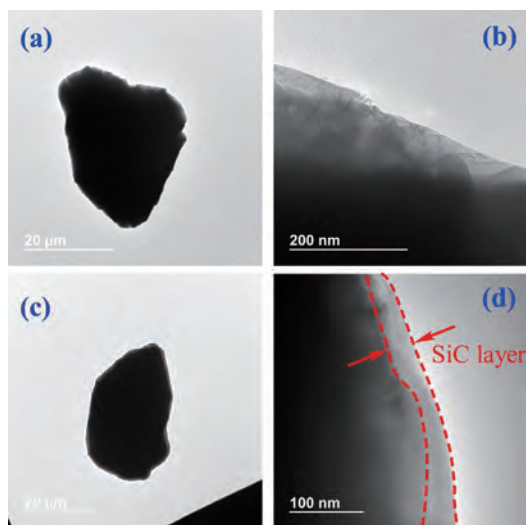


Fig. 1 TEM images of (a, b) Diamond and (c, d) SiC-precipitated Diamond

The as prepared SiC-precipitated Diamond was mixed with WC by hand and consolidated by spark plasma sintering (SPS-210LX, SPS Syntex Inc.) at 1673 to 1973 K under a pressure 70 MPa and a holding time of 5 mins. The more obvious shrinkage of WC-20 vol% Diamond/SiC composites compared to that of WC-20 vol% Diamond was found due to the incorporation of SiC nanolayer. And the shrinkage ended after a holding time of about 60s at a sintering temperature of 1873 K, indicating that the sintering process completed.

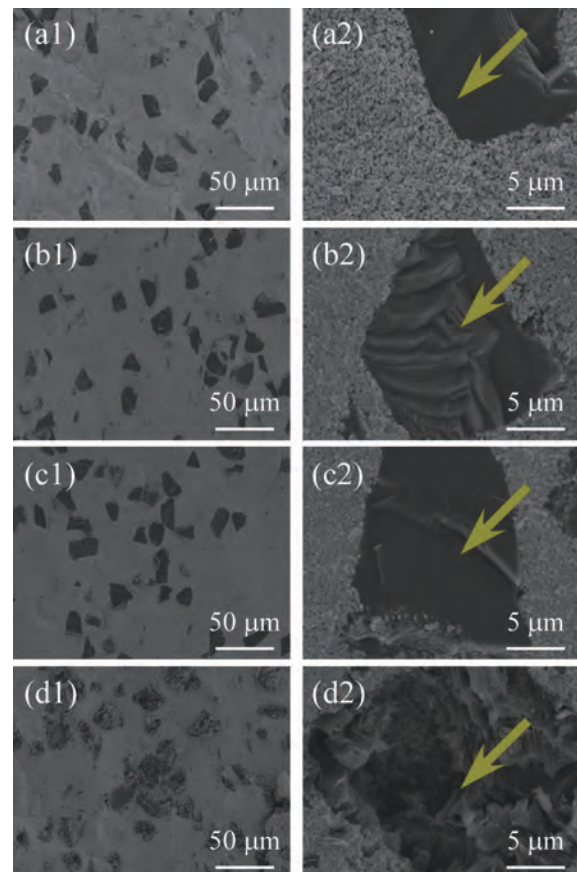


Fig. 2 SEM images of the fracture surface morphology of WC-20 vol% Diamond/SiC sintered at (a1, a2) 1673 K, (b1, b2) 1773 K, (c1, c2) 1873 K, (d1, d2) 1973 K.

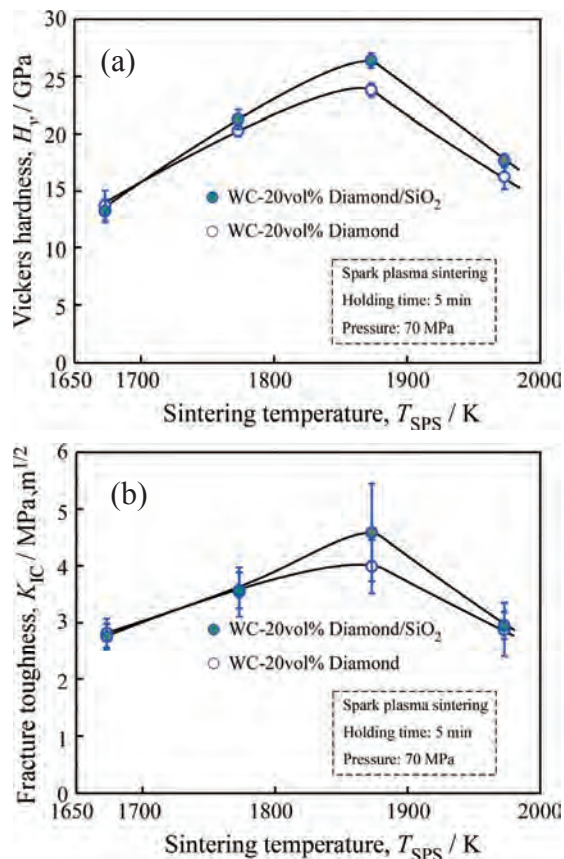


Fig. 3 Mechanical properties of WC-diamond/SiC composites

(a) Vickers hardness, (b) Fracture toughness

The X-ray diffraction patterns indicate that the phase transformation of Diamond started from 1873 K in WC-20 vol% Diamond, but from 1973 K in WC-20 vol% Diamond/SiC indicating the SiC nanolayer coating elevated the phase transformation of Diamond about 100 K.

The SEM images of the fracture surface morphology of WC-20 vol% Diamond/SiC sintered also indicate the beneficial effect of SiC nanolayer coating. At 1673 to 1873 K, the morphology of Diamond kept similar due to the low or even less phase transformation of Diamond. Even at 1973 K, only a little transformation traces can be observed due to the hindering effect of SiC additive.

Just due to the successful incorporation of SiC nanolayer on Diamond, the mechanical properties of WC-Diamond/SiC were apparently improved compared to those of WC-Diamond. As shown in Fig. 3 (a) and (b), the maximum hardness and fracture toughness of WC-20vol% Diamond/SiC composite were 26.4 GPa and 4.59 MPa m^{1/2}, about 3 GPa and 0.6 MPa m^{1/2} higher than those of WC-20vol% Diamond composite, respectively.

References

- [1] M. Kitiwan, H. Katsui, and T. Goto, *Science of Advanced Materials*, 9, 1–6, 2017
- [2] J. Zhang, H. Katsui, Z. He and T. Goto, *J. Asian. Ceram. Soc.* 2, 204–209, 2014.
- [3] J. Zhang, R. Tu and T. Goto, *Journal of the European Ceramic Society*, 34, 435–441, 2014

Keywords: Powder coating; Diamond; Spark plasma sintering; Phase transformation
 Jianfeng Zhang, College of Mechanics and Materials, Hohai University,
 Xikang Road-1, Nanjing 210098, P.R. China
 E-mail: jfzhang@hhu.edu.cn

Epitaxial growth of GaN on ScAlMgO₄ substrates

GaN layers grown on sapphire still suffer from copious dislocation arising from the huge (13%) lattice mismatch between the substrate and overgrowth. ScAlMgO₄ substrates offer a mismatch of only 1.8% and an atomically-smooth growth surface free of polishing damage obtained by cleaving. One of the main challenges in this approach is the incorporation of impurities in the overgrown films, particularly Mg, from the substrate. The aim of this work was to reduce dislocations and control the unwanted impurities.

High-quality GaN films can be epitaxially grown on ScAlMgO₄ (SCAM) (0001) substrates by metalorganic chemical vapor deposition (MOCVD) due to a small lattice mismatch between GaN and SCAM, which is only 1.8%. In addition, scam crystal can be easily cleaved along the (0001) planes, offering an atomically smooth surface free of polishing damage.

However, even 1.8% lattice mismatch still results in copious dislocations and strain the GaN epitaxial films. Therefore a new growth route was devised whereby first a GaN film is grown at high supersaturation to a thickness of about 200 nm, resulting in 3D pyramidal islands, and then transitioned to a lower supersaturation growth mode, by either increasing growth temperature or decreasing V/III ratio, to smoothen the growth surface. This process further reduces dislocation density by one or two orders of magnitude and reduces in-plane strain.

Strain relaxation is practically impossible on the c-plane GaN due to unavailability of adequate slip systems while the low index pyramidal facets of GaN provide many such slip systems. This relaxation process is shown as an illustration in the cross-sectional image in Figure 2, where GaN pyramids were grown to relax AlGaIn films with a similar mismatch as encountered in the growth of GaN on SCAM. In this process, a SiO₂ layer of approximately 40 nm thickness was deposited on a GaN substrate and the oxide film was patterned by RIE etching leading to 2 μm wide openings. Subsequently, a GaN layer was grown by MOCVD on this substrate at high supersaturation, resulting pyramids, which provide relaxation planes for the overgrown AlGaIn. When an AlGaIn is grown on these planes, misfit dislocations form at the AlGaIn/GaN interface leading to relaxation of the AlGaIn film and allowing for growth of nearly strain-free thick epitaxial layers. As the last step, AlGaIn is grown at low supersaturation to promote lateral growth and flattening of the surface. After a fully coalesced AlGaIn film is grown, a strain-free device structure can be grown on it.

In Figure 2, the SiO₂ mask layer can be seen as the dark stripes at the interface between the substrate and the epitaxial layers. The two different grey tones of the GaN pyramids are related to different oxygen incorporation (and as a result different conductivity) in these regions,

which are due to growth in two different crystallographic directions, c and r. For the AlGaIn layer that was grown on the GaN pyramids, two grey tones are observed as well: First, a diamond shaped layer is grown on the pyramidal facets of GaN, which is then followed by coalescence and growth of a homogenous AlGaIn layer. The diamond shaped region has a different Al-content than the topmost layer. This behavior again arises from the growth in different crystallographic directions.

These results show, that the proposed strategy for growth of GaN on SCAM could be templates for growth of device structures of exceptional quality.

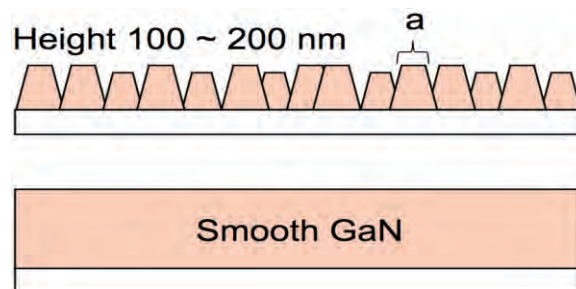


Figure 1: Schematic of the two step growth process for further reduction of dislocations: (top) pyramidal growth at high supersaturation bends dislocation toward the free surface and (bottom) subsequent growth at low supersaturation promotes lateral growth, which aids in dislocation annihilation and formation of a flat surface.

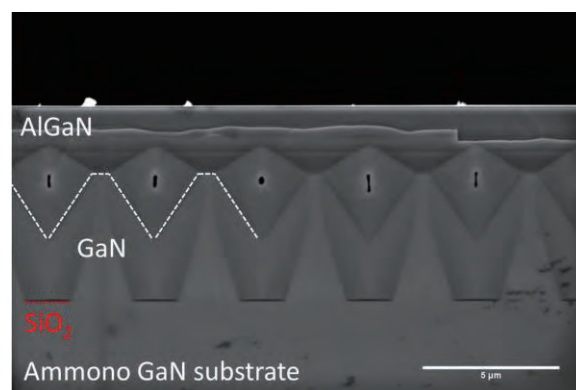


Figure 2: Cross-sectional Scanning electron micrograph of AlGaIn grown on GaN using the relaxation scheme described above. The growth of GaN pyramids is outlined in white.

Keywords: GaN, MOVPE, ScAlMgO₄,
Full Name (Zlatko Sitar, North Carolina States University)
E-mail: sitar@ncsu.edu (Zlatko Sitar), matsuoka@imr.tohoku.ac.jp (Takashi Matsuoka)
<http://www.imr.tohoku.ac.jp/>

Activity Report

Integrated Projects



FY2016-2017 Integrated Projects

No.	PI	Host	Proposed Research	Title	Affiliation	Term
16PJT01	Prof. Awaji	Xavier Chaud	Developments of RE123 Insert Magnet	Research Engineer	Laboratoire National des Champs Magnétiques Intenses, CNRS, France	FY2016-2017
16PJT02	Prof. Kato	Eric Maire	Investigation of Structure and Properties of Nanoporous Metals Formed by Dealloying in Metallic Melt	Research Director	Institut National des Sciences Appliquées de Lyon, France	FY2016-2017

Developments of RE123 insert magnet

We performed quench analysis and R&D tests of high temperature superconducting insert magnets for future high field magnet beyond 30 T using REBa₂Cu₃O_y (RE123, RE: rare earth). The quench properties of the 25T cryogen-free superconducting magnet (25T-CSM) was simulated by the finite element method. We found a solution of quench protection of RE123 insert coil, which is recognized as one of serious issues of HTS magnet.

We successfully achieved a high magnetic field of 24.6 T in a 52 room temperature bore using a 25T cryogen-free superconducting magnet (25T-CSM) [1]. The 25T-CSM now operates as a user magnet at High Field Laboratory for Superconducting Materials (HFLSM) and makes a significant contribution to high field researches. Now the HFLSM in Sendai, Japan and Laboratoire National des Champs Magnétiques Intenses (LNCMI) in Grenoble, France are developing 30 T superconducting magnet. The collaboration of both laboratories focuses on the high temperature superconducting magnet technology.

The high field generation of 24.6 T of the 25T-CSM was made with the Bi₂Sr₂Ca₂Cu₃O_y (Bi2223) insert. In order to develop high field superconducting magnet beyond 30 T, however, the REBa₂Cu₃O_y (RE123, RE=rare earth) insert magnet should be used because its high performances of in-field critical current density and mechanical properties. The most serious problems of RE123 insert are a quench protection and a mechanical behavior of the coil under a huge electromagnetic stress. In this project, we focus on those subjects using simulation and experiments.



Fig. 1 Photo and coil image of 25T-CSM

Fig.1 shows the photo and coil images of the 25T-CSM. From the test of RE123 insert coil in the 25T-CSM, we confirmed that the quench protection circuit was effective at least for 6 s after the quench but the sudden drop of coil operation current took place at 6 s. Using the simulation based on the Comsol, developed at Grenoble, we succeeded in the reproduction of the quench behavior of the 25T-CSM. According to the simulation results, the temperature of a part of the RE123 insert coil reaches around 600 K at 6 s after the quench detection dumping as shown in Fig. 2. However, we found the solution to protect the coil from the damage by the simulation. It should be applied for the protection design of the 30 T-CSM.

For development of a 30T cryogen-free superconducting magnet, we made and tested a RE123 pancake coil with co-winding double-stacked RE123 tapes as shown in Fig. 3. We succeeded in the stable operation of the coil with large stress states up to 580 MPa, which is larger than 490MPa required for the 30 T-CSM. At the same time, we found that an electromagnetic coupling of double-stacked tapes influences the magnetic field and dissipation of the coil. It causes the magnetic field instability and ac losses of the coil.

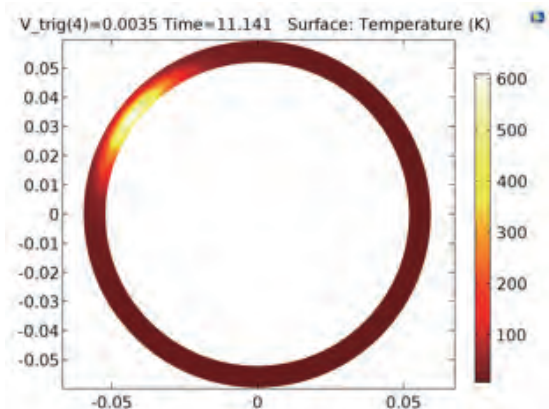


Fig. 2 Simulation result of temperature distribution in a part of RE123 insert coil of the 25T-CSM at 6s after the quench detection. The quench detection voltage is 3.25mV.

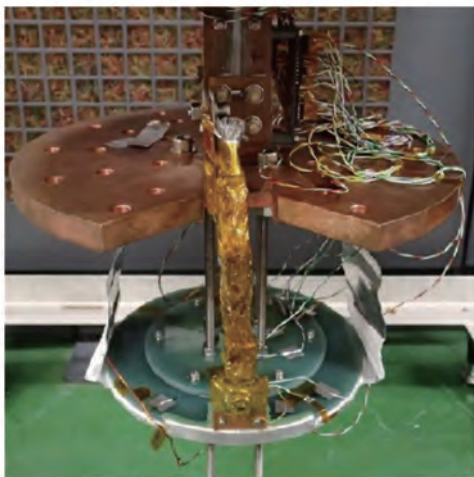


Fig. 3 Photos of (Top) double-stacked RE123 tape co-wound coil at Tohoku University and (Bottom) single tape wound RE123 coil at LNCMI.

The LNCMI performed the test of their own RE123 coil using $\phi 360\text{mm-8T-CSM}$ at the HFLSM. It is for NUGAT project at LNCMI, which is to develop a 10 T RE123 insert coil operated in a background field of 20 T by the water cooled resistive magnet. The magnetic field of 1.3 T under the background field of 8 T was confirmed with an electromagnetic stress of 205 MPa. In particular, the coupling of the RE123 insert to the outer low temperature superconducting magnet was observed, when the outer LTS magnet quenched. We found that the induced current reaches to about 80% of operation

current. The protection circuit should be designed so that the induced current in the RE123 coil is less than critical current.

The critical current density properties of RE123 tapes are also quite important for the high field magnet. We also evaluated them in detail in high magnetic fields up to 24 T. The flux pinning model of RE123 tapes with artificial pinning center (APC), which is recently used for the practical RE123 tapes, were proposed [3]. It can explain the complicated critical current density properties of RE123 with APC.

The 5th French-Japanese high field workshop (F-J WS) was held on December 17-20, 2017 at Tsukuba and Sendai. Six French and fifteen Japanese researchers attended to the workshop at this time. The important topics such as quench protection, shielding current and RE123 coil fabrication method were discussed in detail. The continuous collaboration between LNCMI, NIMS and HFLSM was confirmed for high field magnet developments using high temperature superconducting materials.

In summary, we found the quench protection method of RE123 insert coil, which is recognized as one of serious issues of HTS magnet by the simulation and experimental. The R&D RE123 insert coils were fabricated and tested under the background field of large bore superconducting magnets at HFLSM. We found the solution of quench protection of RE123 insert coil. We confirmed the international collaboration between France and Japan for high field magnet development should be continued.

References

- [1] S. Awaji, K. Watanabe, H. Oguro, H. Miyazaki, S. Hanai, T. Tosaka, S. Ioka, *Supercond. Sci. Technol.* 30, 065001 (2017).
- [2] T. Benkel, N. Richel, A. Badel, X. Chaud, T. Lecomte, F. Borgnolutti, P. Fazilleau, K. Takahashi, S. Awaji, P. Tixador, *IEEE Trans. Appl. Supercond.*, 27, 4602105 (2017).
- [3] S. Awaji, Y. Tsuchiya, S. Miura, Y. Ichino, Y. Yoshida, K. Matsumoto, *Supercond. Sci. Technol.* 30, 1140005 (2017).

Keywords: High magnetic field, superconductivity
Satoshi Awaji (High Field Laboratory for Superconducting Materials)
E-mail: awaji@imr.tohoku.ac.jp
<http://hflsm.imr.tohoku.ac.jp>

Investigation of Structure and Properties of Nanoporous Metals Formed by Liquid Metal Dealloying

Liquid metal dealloying (LMD) technique allows us to prepare fine porous materials with base metal elements, which is principally difficult by the conventional chemical dealloying techniques. In this study, mechanism of morphology formation during LMD was studied by SEM, XRD, EBSD and X-ray and electron tomography.

Nanoporous metals have attracted considerable attention for their excellent functional properties^[1]. The most promising technique used to prepare such nanoporous metals is dealloying in aqueous solution. Nanoporous noble metals including Au have been prepared from binary alloy precursors^[2]. The less noble metals, unstable in aqueous solution, are oxidized immediately when they contact water at a given potential so this process is only possible for noble metals. Porous structures with less noble metals such as Ti or Fe are highly desired for various applications including energy-harvesting devices^[1]. To overcome this limitation, a new dealloying method using a metallic melt instead of aqueous solution was developed in Kato lab^[3]. Dealloying in the metallic melt is a selective dissolution phenomenon of a mono-phase alloy solid precursor: one component (referred as soluble component) being soluble in the metallic melt while the other (referred as targeted component) is not. When the solid precursor contacts the metallic melt, only atoms of the soluble component dissolve into the melt inducing a spontaneously organized bi-continuous structure (targeted+sacrificial phases), at a microstructure level. This sacrificial phase can finally be removed by chemical etching to obtain the final nanoporous materials. Because this is a water-free process, it has enabled the preparation of nanoporous structures in less noble metals such as Ti, Ni, Si,

Fe, Nb, Co and Cr^[4].

In this study, researchers from IMR Japan and INSA Lyon France made collaboration to clarify the mechanism of morphology formation during LMD process by taking the advantage of material preparation technique of IMR and material characterization technique of INSA Lyon. In IMR, porous materials were elaborated by the LMD process and microstructure, phase, compositional change was studied. IN INSA Lyon, morphology of the porous materials was three dimensionally studied *in-situ* and *ex-situ* by using X-ray or electron tomography. The analyses were performed on the two typical porous materials, microporous Fe-Cr alloy and nanoporous Si that were promising materials for electrodes, catalysts, supports and filters.

(1) Porous Fe-Cr alloys^[5]

The all samples used in this work were prepared in Kato lab., IMR, Japan. The $(\text{Fe}_{80}\text{Cr}_{20})_{30}\text{Ni}_{70}$, $(\text{Fe}_{80}\text{Cr}_{20})_{50}\text{Ni}_{50}$ and $(\text{Fe}_{80}\text{Cr}_{20})_{70}\text{Ni}_{30}$ precursors ingots were prepared and they were dealloyed 1h at 1093K in a Mg melt bath under a high-purity He atmosphere, which resulted in the formation of Fe-Cr/Mg bicontinuous structure.

The selective etching step was carried out using highly concentrated nitric acid to dissolve the bath component of Mg, resulting in microporous $\text{Fe}_{80}\text{Cr}_{20}$. Porous sample obtained from $(\text{Fe}_{80}\text{Cr}_{20})_{30}\text{Ni}_{70}$, $(\text{Fe}_{80}\text{Cr}_{20})_{50}\text{Ni}_{50}$ and $(\text{Fe}_{80}\text{Cr}_{20})_{70}\text{Ni}_{30}$ precursor

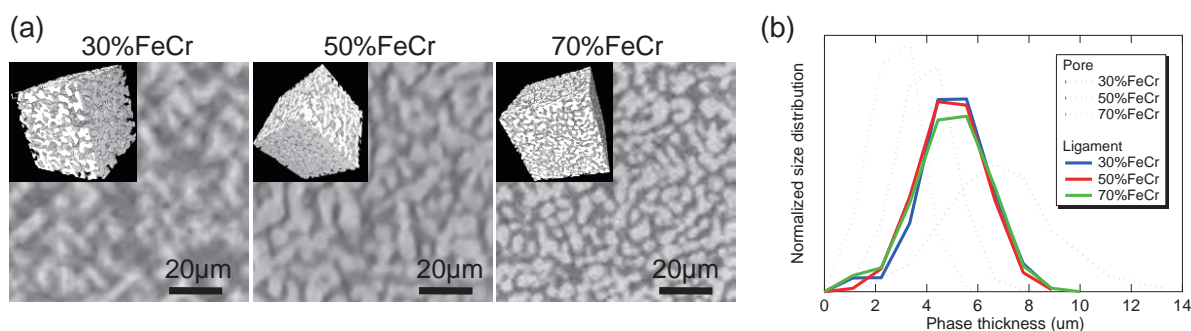


Fig. 1 (a) Images extracted from X-ray tomography scan and 3D view in inset (b) phase thickness distribution^[5]

will be referred as respectively 30%FeCr, 50%FeCr and 70%FeCr. The morphology and microstructure of samples were characterized three dimensionally by X-ray tomography apparatus in MATEIS lab., INSA Lyon, France.

Figure 1(a) shows one reconstructed slice for each sample extracted from the reconstruction and a 3D in inset. Two phases are visible. The lighter phase corresponds to the Fe-Cr phase and the darker phase to the air. From these images morphological parameters can be extracted. Figure 1(b) presents the phase thickness distributions of the Fe-Cr and Air phases for all samples. The phases display a unimodal thickness distribution. The Fe-Cr phase thickness distribution are similar for all samples : i.e. ligaments size are independent of precursor composition. Because Fe-Cr phase thickness distribution are similar and materials density are different, pores distributions must be dependent of precursor composition as shown on Figure 1(b). The average ligaments size is $4.8 \pm 0.3 \mu\text{m}$ for 1h dealloying at 1093K and this value depends only of dealloying time and temperature.

(2) Nanoporous Si for lithium ion battery^[6]

Si is one of the promising material for Lithium ion battery anode. It has theoretical capacity 10 times larger than that of currently used carbon based anode. However, Si anode experiences large volume change upon Li intercalation and self-fractured, resulting in poor cyclic performance. In the previous work, it was found that nanoporous structure greatly improved cyclic performance of Si anode. For understanding the reason for the improvement, the structure of nanoporous Si was analyzed by using electron tomography. The porous Si was prepared by LMD process employing Mg_2Si precursor and Bi metal bath. Precursor was immersed in Bi bath at the designed temperature and time. The

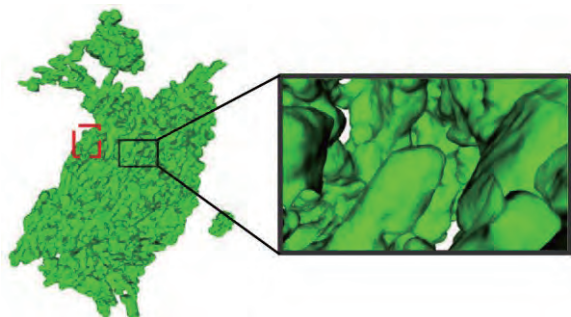


Fig. 2 3D view of nanoporous Si material prepared by LMD treatment using Mg_2Si precursor and Bi metal bath^[5].

representative 3D view of the resulting nanoporous Si is shown in Fig. 2. The 3D images confirm that the aggregates are made of an entanglement of nanorods with a specific surface around $46 \text{ m}^2/\text{g}$ and a large pore volume fraction representing almost half of the total volume of the particles. The Si nanorods systematically exposing the {111} family crystallographic planes at their facets. These are important features because the large porous volume can provide sufficient space for the silicon expansion preventing the fracture or cracking of the Si particles during the lithiation process.

(3) Metallic glass as a precursor of LMD

For LMD precursor, homogeneous single phase solid solution is required because composition fluctuation in the precursor usually results in inhomogeneous porous structure. However, solid solution phase satisfying LMD reaction condition does not always exist in the equilibrium phase diagrams. Metallic glass, a non-equilibrium metal with disordered atomic configuration, is known to have long range structural and compositional homogeneity which can be a precursor for LMD process. In IMR Kato lab., Ti-Zr-Cu-Ni-Pd bulk metallic glass precursors were prepared and it will be used for measuring X-ray tomography *in-situ* in INSA Lyon MATEIS lab., for further understanding the morphology evolution mechanism of the LMD process.

References

- [1] J. Snyder, T. Fujita, M. Chen, J. Erlebacher. *Nat. Mater.*, 9 (2010) 904-907
- [2] A.J. Forty. *Nature*, 282 (1979) 597-598
- [3] T. Wada, K. Yubuta, A. Inoue, H. Kato. *Mater. Lett.*, 65(2011) 1076-1078
- [4] M. Mokhtari, C. Le Bourlot, J. Adrien, S. Dancette, T. Wada, J. Duchet-Rumeau, H. Kato, E. Maire, *J. Alloys Compd.*, 707, (2017), 251–256
- [5] M. Mokhtari, C. Le Bourlot, J. Adrien, A. Bonnin, T. Wada, J. Duchet-Rumeau, H. Kato, E. Maire, *Mater. Charact.* (under review)
- [6] L. Roiban S. Koneti T. Wada, H. Kato, F. J. C. S. Aires, S. Curelea, T. Epicier, E. Maire, *Mater. Charact.* 124, (2017) 165-170

Keywords: porosity, foam, morphology
 Hidemi Kato (Non-Equilibrium Materials)
 E-mail: hikato@imr.tohoku.ac.jp
<http://www.nem2.imr.tohoku.ac.jp/index-e.html>

Activity Report

Workshops



FY2017 Workshops

No.	Chairperson	Title of Workshop	Place	Date
17WS01	Prof. Kato	12th International Workshop on Biomaterials in Interface Science	Akiu, Miyagi	2017.8.4-5
17WS02	Prof. Bauer	International Workshop on New Excitations in Spintronics	Auditorium, IMR	2018.1.10-12
17WS03	Prof. Goto	International Workshop on Ceramic Science and Engineering in Sendai (IWCSE Sendai)	Sakuha Hall, Tohoku Univ.	2018.3.12-14
17WS04	Prof. Saito	KIST- Tohoku University Joint Symposium	KIST	2017.11.21-22

The 12th International Workshop on Biomaterials in Interface Science

- Innovative Research for Biosis-Abiosis Intelligent Interface Summer Seminar 2017 -

Biosis-abiosis intelligent interface science has been developed by interdisciplinary and collaborative works to understand and control phenomena arising at the interface between human constituents and biomaterials. Researchers and students from various fields related to biomaterials gathered at the 12th International Workshop on Biomaterials in Interface Science on Aug. 4–5th at Sendai, Japan. The invited lectures by 7 forefront researchers and 21 contributed papers provided valuable opportunity for cross-over discussion, interdisciplinary idea sharing and new collaboration to develop the intelligent interface science.

To develop advanced biomaterials that can be adopted in human bodies for a short time and be used over a long term, highly functional and autonomic intelligent interface should be created by combining knowledge obtained from various research fields, such as material science, medical engineering and dentistry, since phenomena occurring at the biosis-abiosis interface are quite complicated. Therefore interdisciplinary and international research activities are of great importance to understand the complex phenomena and optimize the biosis-abiosis interface by developing biomaterials, material design and systems. Three Institute in Tohoku University, namely Institute for Materials Research (IMR), Graduate School of Dentistry and Graduate School of Biomedical Engineering, have been collaborating and involved in the 5-year project on Biomaterials to establish a new concept, "Biosis-Abiosis Intelligent Interface Science". In the frame the project, the series of international forums have been held 11 times. For further developing the Biosis-Abiosis Intelligent Interface Science, 12th International Workshop on Biomaterials in Interface Science in conjunction with Innovative Research for Biosis-Abiosis Intelligent Interface Summer Seminar 2017 was held by a new collaborative project "Creation of Life Innovation Materials for Interdisciplinary and International Researcher Development" on Aug. 4th–5th, 2017, at Akiu in Sendai, Japan.

This workshop had 7 invited lectures and 21 contributed papers. The invited lectures were given by distinguished professors on biomaterials from Taiwan, China, Russia, Korea, Mexico and Japan. 81 participants of professors, researchers and students attended. Prof. Kwangmahn KIM, who is the dean of Department and research institute

of dental biomaterials & bioengineering, Yonsei University provided an invited lecture on alternative test methods of biocompatibility test for dental biomaterials. The topic of the invited lecture by Prof. Tzer-Min LEE was on the current status and future of surface treatments of dental implants. Prof. Takao HANAWA gave an invited lecture on next generation implant surface. The state-of-the-art research on in vivo multiscale photoacoustic imaging was provided by Prof. Chulhong KIM. Prof. MANGKONSU gave an invited lecture on sintering behavior of beta-tricalcium phosphate and its properties. Prof. James TSOI introduced dental CAD/CAM materials. From the side of material science, Prof. Torres-Martinez provided a lecture on an efficient photocatalytic material of $\text{Na}_2\text{Zr}_x\text{Ti}_{6-x}\text{O}_{13}$ while Prof. Zadorozhnyy introduced his updated research on biocompatible metal materials produced by severe plastic deformation methods. These invited lectures and contributed papers gave the all participants a valuable opportunity for sharing interdisciplinary viewpoints and ideas. The collaborative discussion had great contributions to the development on the intelligent interface science on biomaterials.



Fig.1 Shots in lectures and Group photo.

Keywords: Biomedical, ceramic, metal
Hidemi KATO (Non-Equilibrium Materials)
E-mail: hikato@imr.tohoku.ac.jp
<http://interface2017.imr.tohoku.ac.jp/>

International Workshop on “New Excitations in Spintronics”

This international workshop was held from 10-14 January 2018 at the Institute for Materials Research of Tohoku University with support from the ICC-IMR.

Tohoku University has been a center of research on the physics of spintronics, i.e. the science and technology to control the charge and spin of the electrons in small structures and devices. Its researchers have profited in the past directly and indirectly from the support by the Reimei program of the ASRC of the JAEA and the Graduate Program on Spintronics (GP-Spin) of Tohoku University. In this workshop, we brought together the different blood groups of spintronics, who otherwise meet only in small groups at specialized workshops focused on a single topic. In particular, we wanted to stimulate exploration of novel ways of extending spintronics by coupling to other excitations, such as magnons, photons, phonons, spinons, cavitrons, excitons, orbitrons, etc. We invited selected researchers from spintronics and related fields in order to share results on the dispersion and lifetimes of such excitations and exchange thoughts and ideas that will lead to improved spintronic devices.

The members of the Program and Organizing Committee have been:

Gerrit Bauer (IMR & WPI-AIMR) [Chair]
Sadamichi Maekawa (JAEA) [Co-Chair]
Yoshiro Hirayama (Tohoku) [Co-Chair]
Tim Ziman (ILL) [Co-Chair]
Joseph Barker (IMR)
Michiyasu Mori (JAEA)
Kentarō Nomura (IMR)
Eiji Saitoh (IMR & WPI-AIMR)
Koji Sato (IMR)
Koki Takanashi (IMR)
Oleg Tretiakov (IMR)
Mika Terada (IMR, secretary)

Details of the scientific program including the abstracts of oral and poster sessions can be found here:

www.bauer-lab.imr.tohoku.ac.jp/reimei2018

The conference statistics are:

Number of Participants	104
Overseas	28
- Australia	1
- China	6
- Czech Republic	1
- France	2
- Germany	8
- Ireland	1
- The Netherlands	7
- USA	2

We are very grateful to the speakers, poster presenters, sponsors, organizing committee, and unnamed students of the IMR Theoretical Physics Group for making the Workshop a resounding success.

Fig. 1 Official NES2018 conference picture

Keywords: spintronics, magnetism, neutron scattering
Gerrit Bauer, Institute for Materials Research, Tohoku University, Sendai, Japan
E-mail: g.e.w.bauer@imr.tohoku.ac.jp
<http://www.bauer-lab.imr.tohoku.ac.jp/>

International Workshop on Ceramic Science and Engineering in Sendai (IWCSE Sendai)

Ceramic science is an interdisciplinary and integrated research field. Without its development, human society cannot make progress. Although ceramics were anciently invented, modern ceramics are advancing rapidly, leading into new fields beyond the conventional image of ceramics. The properties of ceramic materials are strongly affected by processing, and thus a new processing can produce new materials which can trigger significant development of society. We have organized the joint conference (IWCSE Sendai) of ISAC-6, AOCF-7, and Thin Film Workshop in March 12 to 14, 2018 in Sendai, Japan. The invited lectures by fifty-five experts and thirty-two contributed papers provided valuable opportunity for cross-over discussion, interdisciplinary idea sharing and new collaboration to develop and establish the ceramic science and engineering.

The science and technology of ceramics are advancing rapidly, leading into new fields far beyond the conventional image of ceramics. Careful tailoring of micro- and nano-structures is yielding superior mechanical, chemical, and electrical properties. Engineering structural and functional ceramics are expected to find uses as key components in a variety of industrial applications from engines with high efficiency long-term durability to devices to maintain clean environments. The International Workshop on Ceramic Science and Engineering in Sendai (IWCSE Sendai), that is the ICC-IMR workshop, discussed on the advanced monolithic and composite ceramic materials for wide-ranged applications in conjunction with the Japan Society for the Promotion of Science (JSPS) and the Asia-Oceania Ceramic Federation (AOCF) and the Thin Film Society. The JSPS 124th Committee on Advanced Ceramics has been conducting a series of International Symposium on Advanced Ceramics (ISAC). Following the first symposium at Kurume, Japan in 1997 (ISAC-1), Shanghai, China in 2002 (ISAC-2), Singapore in 2006 (ISAC-3), Osaka, Japan in 2010 (ISAC-4), and Wuhan, China (ISAC-5), ISAC-6 was scheduled at Sendai because Tohoku University is one of the most advanced research institution for ceramics. The AOCF has also been conducting a series of international conferences at Osaka, Japan in 2005 (AOCF-1), at Daegu, Korea in 2006 (AOCF-2), at Lijiang, China in 2008 (AOCF-3), at Osaka, Japan in 2010 (AOCF-4), at Jeju, Korea in 2013 (AOCF-5), and at Guilin, China in 2015 (AOCF-6). The Thin Films Workshop is a series of workshop on thin film and surface science, focusing topics related to ceramic coatings. Since the materials science of ceramics is interdisciplinary research field, the ICC-IMR workshop was held with the ISAC-6, AOCF-7 and Thin Films Workshop 2018 on March 12th to 14th at Tohoku University in Sendai.

The 3-days technical program in this workshop include 87 papers in which 55 invited lectures were given by distinguished professors and experts on ceramics from US, UK, Germany, Italy, France, Ukraine, Slovak, Sweden, Brazil, Australia, Singapore, India, Thailand, China, Korea, Taiwan and Japan. The ICC-IMR workshop consisted of 18 sessions discussing on knowledge sharing of state-of-the-art research on advanced functional and structural ceramics with regards to basic material science and practical applications discussing on development of high strength ceramics, composites and porous materials; coating techniques to resist wear, erosion and tribological loadings; new processing of fiber, matrices, interfaces, CMCs; transparent materials; ultra high-temperature ceramics and ternary compounds; tribological behaviors and heat and corrosion resistances of various types of ceramic materials and coatings; developing thermal and environmental barrier coatings; joining and machining of ceramics and composites, mechanics and characterization techniques in order to establish interdisciplinary and international network of scientists leading the ceramic materials



Fig.1 A group photo of the ICC-IMR workshop

Keywords: ceramic, thin film, coating
 Takashi GOTO (Multi-Functional Materials Science)
 E-mail: goto@imr.tohoku.ac.jp
<http://www.isac-6.imr.tohoku.ac.jp/>

KIST-Tohoku University Joint Symposium –Advanced Materials and Devices-

Korea Institute of Science and Technology (KIST) is a long-term partner institute of IMR. Alternating “KINKEN-KIST joint symposium” in Sendai and Seoul are important for connecting each researches by exchanging the idea in the broad range of the materials science. In 2017, “Tohoku University – KIST joint symposium” was held at KIST including the medical fields.

“KIST - Tohoku University Joint Symposium” was held at KIST (Korea Institute of Science and Technology) campus in Seoul on 21-22 November 2017. Tohoku University has a long history of academic exchange with KIST. As a commemoration of concluding university - level academic exchange agreement between KIST and Tohoku University in 2016, Institute for Materials Research (KINKEN) and KIST jointly held a seminar “KINKEN-KIST joint seminar” in Sendai, and that led to this symposium in Seoul in this year. In this Seoul symposium, researchers of Institute for Materials Research and Graduate School of Medicine were joined to open the joint symposium. Two sessions of “Advanced materials and devices” and “ Biomolecular signatures in health care” were held in parallel.

Prof. Sasaki, deputy director of IMR, and seven IMR researchers participated in this symposium from IMR by supporting from ICC-IMR. Starting from Prof. Sasaki's presentation about introduction of IMR, wide range of research topics such as spintronics, crystal growth and nano-porous metal were

presented. From KIST side, broad range of research activities in KIST such as spintronics, organic semiconductor and quantum computer were given. Vigorous discussions were exchanged throughout the symposium. In the next day (22 November), lab tours in Post-silicon Semiconductor Institute (PSI), KIST and group discussions were carried out.

We will deepen an academic relationship with KIST continuously through holding symposium alternately from next year.



Fig. 2 Lecture on “Spin current physics” by Prof. Eizi Saitoh, IMR



Fig. 1 Group photo of Tohoku University - KIST symposium -Advanced materials and Devices

Keywords: spintronics, electronic materials, crystal
Takahiko Sasaki (Low Temperature condensed state physics)
E-mail: takahiko@imr.tohoku.ac.jp

Activity Report

KINKEN WAKATE



FY 2017 KINKEN WAKATE

No.	Chairperson	Title of Workshop	Place	Time
17KW01	Prof. Sasaki	KINKEN WAKTE 2017 "New Frontier of Molecular Materials"	Auditorium, IMR	2017.9.29-30

KINKEN-WAKATE 2017: New Frontier of Molecular Materials

International conference for young researchers, New Frontier of Molecular Materials, were held at IMR auditorium on Sep. 29-30, 2017, as the post-conference of ISCOM2017. More than 60 researchers including students studying molecular materials attended. Three tutorial lectures on physics, theory, and chemistry were given, including 26 oral and 15 poster presentations.

New Frontier of Molecular Materials (NFMM), for young researchers, were held as KINKEN-WAKATE of this fiscal year at auditorium in IMR on Sep. 29-30. Three prominent professors, Prof. M. Dressel for physics, Prof. V. Dobrosavljevic for theory, and Prof. H. Mori for chemistry were invited for tutorial lectures for students and young researchers. Starting with the historical talk about IMR and KINKEN-WAKATE by Prof. H. Fukuyama, 26 oral and 15 poster presentations were made with active and fruitful discussions for the two days. Various discussions among researchers across generations and research fields were held in the evening session currently with poster presentation. The participants included 23 students, 19 young and 11 senior researchers, 8 professors.

There are two purposes of NFMM. One is to provide opportunities of oral presentation for young researchers, and the other is to promote comprehensive understanding of organic material from basic to advanced problems. 26 oral presentations were selected, which were divided into 7 sessions, including various experimental and theoretical works covering almost all the fields in the molecular material science: phase transitions and its control, charge frustrations and its slow dynamics, exotic phenomena such as ferroelectricity, superconductivity, and Dirac electrons, and problems of electronic correlations including π -d and spin-orbit interactions.

Research on molecular materials is roughly divided into three fields: physics, chemistry, and theory. Their close cooperation has greatly contributed to the development of this field. For this reason, prominent lecturers for pedagogical talk were selected to cover many fields. Prof. M. Dressel lectured on the physics of molecular materials from free electron gas to Mott-Hubbard transition with appropriate optical spectrum, including recent topics in correlated electrons system.

Prof. V. Dobrosavljevic lectured on theories used in strongly correlated electron systems, especially for dynamical time scale and special range of interactions with frustrations and randomness comparing with several methods. Prof. H. Mori introduced the chemical properties in relation to hydrogen, which are used in the engineering and sometimes causes problems, including recent discoveries of ferroelectrics due to hydrogen bonding and its fluctuations.

Prof. B. Powell provided the summarized talk of the conference, in which many suggestive insights were given for the young researchers referring to old and newly discovered problems, advantages and disadvantages in the field, and perspectives. With closing remarks by Prof. J. Müller, the conference ended successfully.



Fig. 1 Group photo in front of the building 2 in IMR.

References

- [1] URL of NFMM web site:
<http://www-lab.imr.tohoku.ac.jp/~nfmm/index.html>

Keywords: organic, electrical properties,
 Satoshi Iguchi (Low Temperature Condensed Matter Physics Division)
 E-mail: satoshi.iguchi@imr.tohoku.ac.jp
<http://cond-phys.imr.tohoku.ac.jp/index.html>

Activity Report

Short-term Visiting Researchers



FY 2017 Short-term Visiting Researchers

Application No.	Name	Host	Proposed Research	Title	Affiliation	Term
17SV01	Atsufumi Hirohata	Prof. Takanashi	Experimental Demonstration of a Persistent Current	Professor	University of York, UK	2018.3.14-3.25
17SV02	Wan Faron	Prof. Nagai	Study of Strength Factor in Multi-Scale Model for Neutron-Irradiated Materials by Means of Nano-Micro Specimen Technology	Professor	University of Science and Technology Beijing, China	Prof. Zhan Qian Prof. Chang Yongqin 2017.7.17-7.31
17SV03	Wan Jun Jiang	Prof. Takanashi	Exploration of Magnetic Skyrmions in Heusler Alloy Based Multilayer	Assistant Professor	Tsinghua University, China	2017.7.22-8.5
17SV04	Hatem Zurob	Prof. Furuhashi	Alloying Effects on Ferrite / Austenite Interface Migration in Ferrous Alloys	Professor	McMaster University, Canada	2017.11.8-11.17
17SV05	Subhankar Bedanta	Prof. Takanashi	Study of Spin Transfer Torque in $\text{Co}_2\text{Fe}_x\text{Mn}_{1-x}$ Si Heusler Alloy	Associate Professor	National Institute of Science Education and Research (NISER), India	2017.7.8-7.22
17SV06	Sergei Zvyagin	Prof. Nojiri	Probing Spin Dynamics in Frustrated Spin Systems under Pressure: High-Field ESR	Scientist	Dresden High Magnetic Field Laboratory, Helmholtz-Zentrum Dresden-Rossendorf, Dresden, Germany	2017.9.3-9.12
17SV07	Georges Boulon	Prof. Yoshikawa	Comprehensive Study of Transparent Ceramic and Single Crystal for Scintillator	Emeritus Professor	Claude Bernard University of Lyon 1, France	2018.2.9-2.24
17SV08	Yan-Zhen Zheng	Prof. Nojiri	Potential Single-Molecule Torroics States in Coordination Wheel	Professor	Frontier Institute of Science and Technology, Xi'an Jiaotong University, China	Dr. Yon-Song Ding Ph.D candidate Mr. Hao-Lan Zhang 2018.3.24-3.30
17SV09	Jaewon Choi	Prof. Nojiri	Synchronized Magnetic Field and X-Ray Pulses to Study Quantum Matter in Extreme Conditions	Postdoctoral Researcher	Physik-Institut, University of Zurich, Switzerland	Dr. Jaewon Choi Din Technical Staff Mr. Dominik Rechsteiner 2018.2.17-2.26

Experimental demonstration of a persistent current

Generation of a spin-polarized persistent current in a non-magnet is investigated by introducing a non-uniform magnetic field from an epitaxial FePt nanopillar with perpendicular magnetic anisotropy. Such a spin-polarized persistent current has been theoretically proposed almost 20 years ago [1] but it has not been experimentally demonstrated to date. A device with such a current is expected to open up new research horizons as a spin source for quantum computation.

The quantum phases of charged particles in mesoscopic structures have been investigated intensively. Their interference and oscillatory behaviors have been induced by application of an external field [2]. Electrons traveling along semiconductor or normal metal rings threaded by a magnetic flux acquire a quantum dynamical phase that produces interference phenomena such as the Aharonov-Bohm (AB) [3], Aharonov-Casher [4] and Altshuler-Aronov-Spivak (AAS) effects [5]. In addition, An electron acquires an additional phase element known as the geometrical or Berry phase when the spin of the electron rotates during its orbital motion along the ring-shaped path.

Two sets of devices for the demonstration of a spin-polarized persistent current were fabricated using a new method. An epitaxial ferromagnetic FePt film was grown on a MgO(001) substrate by ultrahigh vacuum sputtering, followed by patterning into a nanopillar with the diameter of 120, 180, 220 and 270 nm in design by a combination of electron-beam lithography and Ar-ion milling. A polycrystalline non-magnetic Ag film was then grown and patterned into a nanoring with the inner diameter of 200, 260, 300 and 350 nm and the width of 100 nm in design in a similar manner. One set has 10 FePt nanopillars in a series with two electrical contacts on each end, allowing to measure the summation of spin-polarized persistent current generated by the 10 nanopillars [see Figs. 1(a) and (b)]. Another set has 1 nanopillar as we fabricated earlier [see Figs. 1(c) and (d)] as a reference.

These devices were measured using a four-terminal method, typically showing between 160 and 260 Ω . We then measured the devices at the Toshiba Cambridge Research Laboratory and found that the resistance is increased by almost 50%.

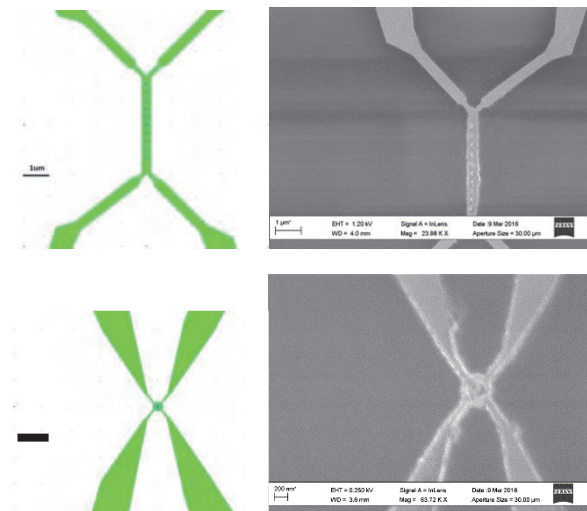


Fig.1 (a) Schematic diagram of 10 FePt nanopillar device with (b) the corresponding scanning electron micrograph (SEM). (c) Schematic diagram of 1 FePt nanopillar device with (d) the corresponding SEM.

In summary, we successfully fabricated and characterized a new quantum device consisting of a ferromagnetic FePt nanopillar enclosed by a nonmagnetic nanoring. We found the devices were very fragile against static charge. We plan to continue to fabricate these devices with a thicker and more robust electrodes to experimentally detect the spin-polarized persistent current.

References

- [1] D. Loss and P. M. Goldbart, *Phys. Rev. B* **45**, 13544 (1992).
- [2] Y. Imry, *Introduction to Mesoscopic Physics* (Oxford Univ. Press, Oxford, 1997).
- [3] K. Sekiguchi *et al.*, *Phys. Rev. B* **77**, 140401(R) (2008).
- [4] F. Nagasawa *et al.*, *Nature Commun.* **4**, 2526 (2013).
- [5] B. Pannetier *et al.*, *Phys. Rev. B* **31**, 3209(R) (1985).

Keywords: spin current, magnetoresistance (transport) and nanostructure
 Atsufumi Hirohata (University of York, United Kingdom)
 E-mail: atsufumi.hirohata@york.ac.uk
<http://www-users.york.ac.uk/~ah566/>

Study of Strength Factor in Multi-scale Model for Neutron-irradiated Materials by means of Nano-micro Specimen Technology

Improved radiation resistance was found in 9Cr-2W steel with 0.1% Si after neutron irradiation. The microstructure, mechanical properties and positron annihilation behavior were studied systematically. Lower number of loops and higher number of nano-precipitates were formed in with Si. It suggests the resistance could be caused by more sinks and defect interaction.

9Cr-2W low activation ferritic steel is one of candidate for the first wall structure materials in fusion reactor system. This series of steels have been developed in Kyoto U, and surveyed several points, especially on effect of Si addition and low temperature embrittlement [1]. AFM-A(w/Si) and AFM-B(w/o Si) were neutron-irradiated in JMTR to 5×10^{23} n/m² at 290°C (1,178 hr, 99M-14U, #2342). The cooling time was 15 years. Under ICC program, Post Irradiation Experiment (FIB, AC-TEM, Tensile test, Nano-hardness test) was carried out at IMR Oarai Center, except positron CBD measurement at Kyoto U.

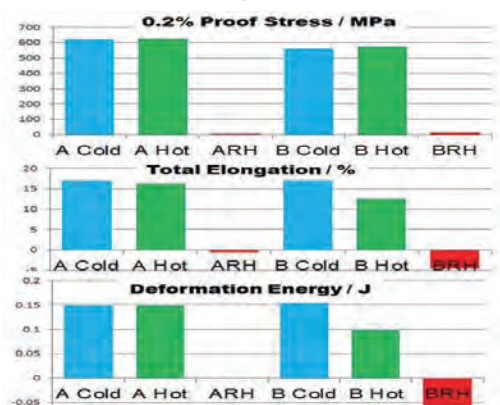


Fig. 1. Yield stress, elongation and deformation energy before and after irradiation. B showed intensive radiation embrittlement.

Fig. 1 shows yield stress, elongation and deformation energy before and after the irradiation, where red bars show induced hardening, elongation loss and reduction of the energy. Comparing with AFM-A (w/ Si) and AFM-B (w/o Si), Si addition improved in radiation-hardening very clearly, because of small hardening and elongation loss.

As shown in fig 2, many black dots were observed in both materials by TEM. By precise observation those black dots were confirmed as radiation induced dislocation loops with 5 nm level. In the comparison, higher density of loops were founded in AFM-B. The result indicates the addition of Si

improve the irradiation resistance due to

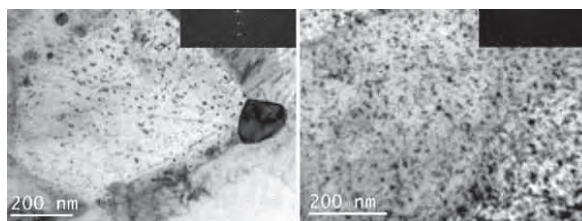


Fig. 2. Black dots formed in AFM-A (w/ Si) and AFM-B (w/o Si).

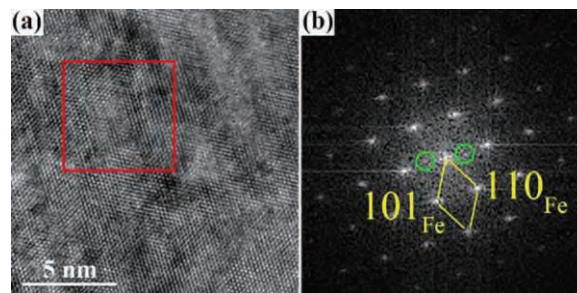


Fig. 3. HRTEM image of with Si sample and FFT image of red box. It suggests nano-precipitate of G phase.

enhancement of internal sinks and defect trapping.

Fig. 3 shows HRTEM and IFFT images from AFM-A (w/o Si). The distances of $(110)_{Fe}$ and $(210)_{Fe}$ calculated via FFT image. The spots with green circle are not belonging to the reciprocal lattice of alpha-Fe. Moreover, PA CBD showing a phase separation occurred. We assume these are G phase with 2-3 nm, at this moment [2]. Thus, keeping an appropriate amount of Si is helpful to improve the resistance to neutron irradiation damage. Several papers will be published in near future.

References

- [1] A. Kimura, et. al., J. Nucl. Mat., 283-287 (2000) 827.
- [2] Y. Matsukawa, et. al. Acta Mat. 116 (2016) 104e113

Keywords: radiation damage, neutron irradiation, strength
 WAN Farong (University of Science and technology Beijing)
 E-mail: wanf@mater.ustb.edu.cn
<http://en.ustb.edu.cn/Research/ShowArticle.asp?ArticleID=244>

Possible stabilization of room-temperature skyrmions in Heusler alloy based magnetic multilayers

Magnetic skyrmions are chiral spin textures that exhibit a great potential for the future spintronic data storage by providing nonvolatile, nanoscale and low-power energy consumption information carriers. Searching of novel skyrmion materials with desired properties thus constitutes as one of the major trends in spintronics which motivates the present study. In this collaboration work, we explore the realization of skyrmion in Heusler alloy based multilayers with ultra-low damping that could result in efficient electric manipulation.

Strong spin-orbit interaction together with broken inversion symmetry gives rise to many exciting physics [1]. Magnetic skyrmions and current induced spin-orbit torques are representative examples[1-3]. The material system along these directions is typically heavy metal/ultrathin ferromagnet/insulator trilayer in which the strong spin-orbit interaction of heavy metal provides (a) a source of interfacial noncollinear Dzyaloshinskii-Moriya interaction (DMI) that stabilizes chiral domain wall/skyrmion and (b) a source of spin currents/spin-orbit torques that enables efficient electrical manipulation. Typical magnetic multilayers are made of ultrathin Co and CoFeB in adjacent to Pt, W, Ir and Ta which exhibit relatively high intrinsic damping, in addition to the extra interfacial contribution to damping. Owing to the low intrinsic damping, Heusler alloy and MnGa based single-crystalline multilayers are currently attracting attention from the community which motivates the present study. Specifically, Heusler alloy and MnGa based materials were explored for simultaneously realizing nanoscale densely packed skyrmion lattices with the size approaching 50 nm, and efficient electrical manipulation produced by the current induced spin-orbit torques as a result of low magnetic damping. These aspects are the heart of the current skyrmion based spintronics research. Realizing of which could pave the pathway towards future functional skyrmion racetrack memory devices. It could also enable room temperature emergent topological spin transport to be investigated, such as topological Hall effect, skyrmion Hall effect and their reciprocity.

Using ultra-high vacuum magnetron sputtering technique, Pt/MnGa/MgO, Pt/FePt, Pt/Co₂(Fe_{0.4}Mn_{0.6})Si/MgO, multilayers with various thicknesses of each layer were synthesized which were done in

collaboration with Prof. Koki Takanashi. Selected results on MnGa based magnetic multilayer are shown in Fig 1.

Fig.1 shows magnetic hysteresis loops measured in-plane and perpendicular to the plane in a MgO / Cr (2) /Pt (3) / MnGa (3) / MgO (2) / Ta (2) multilayer (unit in nm) that was annealed at 300 °C for 1 hour. The presence of perpendicular magnetic anisotropy is clearly presented which is more promising for realizing room-temperature skyrmions. The strength of DMI and damping parameters are currently being examined using Brillouin light scattering (BLS) and FMR techniques, respectively. Associated films were also deposited onto TEM membrane for identifying skyrmion phase in real space by using Lorentz TEM in collaboration with Dr. Ying Zhang (IOP, CAS).

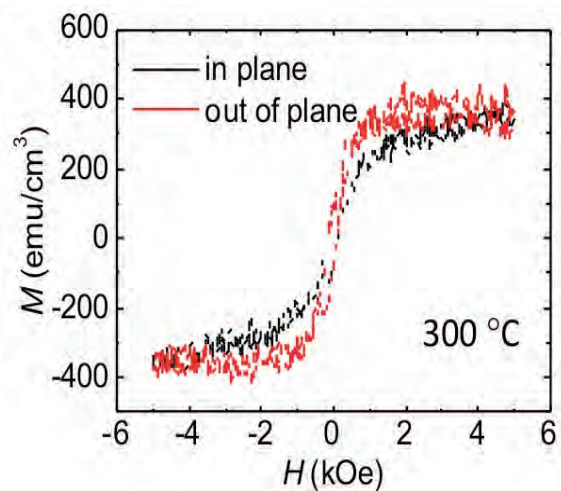


Fig. 1 Magnetic hysteresis loops measured in Pt 3 nm / MnGa 3 nm / MgO 2 nm / Ta 2 nm.

References

- [1] F. Hellman, et al., Rev. Mod. Phys. 89, 025006 (2017).
- [2] W. Jiang, et al., Physics Reports. 70, 1-49 (2017).
- [1] J. Sinova, et al., Rev. Mod. Phys. 87, 1213 (2015).

f Keywords: ferromagnetic, spin current, spintronic
Wanjun Jiang, Department of Physics, Tsinghua University, Beijing, China
E-mail: jiang_lab@tsinghua.edu.cn
<http://www.phys.tsinghua.edu.cn/>

Alloying Effects on Ferrite / Austenite Interface Migration in Ferrous Alloys

A systematic investigation of alloying element segregation to migrating ferrite/austenite interfaces was carried out using Atom Probe Tomography (APT). The investigation included ternary Fe-C-X (X=Mn, Si, Cr, Mo, Ni) and quaternary Fe-C-Mn-Y (Y=Si, Mo) alloys. A nitrogen based alloy, Fe-N-Mn, was also investigated. The results indicate that the interaction between C and the substitutional elements strongly affects the segregation of these elements to the interface.

The interaction of alloying elements with a moving interface has a strong influence on the interface mobility and the overall phase transformation kinetics. This is particularly the case during ferrite precipitation from austenite. In this work, high purity Fe-C-X and Fe-C-Mn-Y alloys were decarburized to produce a random ferrite/austenite interface which is moving at very low velocity. A focused ion beam microscope was used to liftout APT tips from the interface. APT testing was performed using a CAMECA local electrode atom probe operated under laser pulsing mode.

Quantitative analysis of solute segregation led to several important conclusions. In particular, strong carbon segregation was reported at all interfaces. The carbon level at the interface was usually in the range of 6 to 10 at%. In contrast, weak N segregation was observed at interfaces in Fe-Mn-N. The high concentration of C at the interface along with the strong interaction of C with elements like Mn and Si, strongly influenced the segregation of these elements to the interface. In the case of Fe-C-Mn, moderate Mn segregation was observed as shown in Fig. 1. In contrast, no Mn segregation was observed in a similar Fe-N-Mn alloy under identical growth conditions. This seems to enforce the argument that Mn segregation to ferrite/austenite interfaces during ferrite growth is enhanced by the presence of C at the interface and the attractive C/Mn interaction [1]. It is speculated that the wide segregation profiles observed in Fig. 1 are partly due to the fact that Mn segregation is dominated by the interaction of Mn with C at the interface and not by the interaction of Mn with the interface itself. In the case of the Fe-C-Si system, Si segregation was not observed at the interface [2]. This is believed to be due to the strong repulsive interaction between Si and C. In the case of elements that interact strongly with the interface, such as Mo, the segregation profiles were narrower and the segregation levels were similar to those observed at grain boundaries [3].

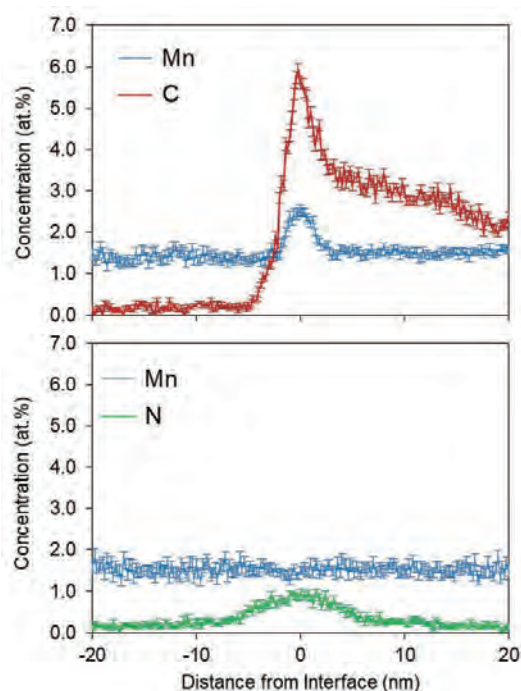


Fig. 1 Comparison of the Mn segregation to ferrite/martensite (formerly austenite) interfaces in Fe-C-Mn and Fe-N-Mn alloys [1].

References

- [1] B. Langelier et al., *Microsc. Microanal.* 23, 385 (2017).
- [2] H.P. Van Landeghem et al., *JOM*, 68, 1329 (2016).
- [3] H.P. Van Landeghem et al., *Acta Mater.*, 124, 536 (2017).

Keywords: Kinetics, Phase Transformations, Steel.

Hatem S. Zurob, Department of Materials Science and Engineering, McMaster University, Canada.

E-mail: zurobh@mcmaster.ca

<http://mse.mcmaster.ca/zurob/>

Study of Spin Transfer Torque in $\text{Co}_2\text{Fe}_x\text{Mn}_{1-x}\text{Si}$ Heusler Alloy

The generation of pure spin current (J_S) and its effect on the switching of the magnetization by spin transfer torque via spin orbital torque have been subject of vivid research in last one decade [1]. The efficient switching of magnetization via spin current depends on the damping properties of the magnetic materials. $\text{Co}_2\text{Fe}_x\text{Mn}_{1-x}\text{Si}$ (CFMS) has a low damping coefficient, therefore, we prepared bilayers $\text{MgO}(100)/\text{CFMS}$ (20 nm)/Pt ($t_{\text{Pt}} = 3, 5, 7, 10, 20$ nm) for the investigations of spin pumping and inverse spin Hall effect (ISHE).

Thin films of CFMS are grown on $\text{MgO}(100)$ substrates using magnetron sputtering. The sample structure was MgO/CFMS (20 nm)/Pt ($t_{\text{Pt}} = 3, 5, 7, 10, 20$ nm). The growth of CFMS thin films were epitaxial on the MgO substrate, which was confirmed *in situ* using reflection high energy electron diffraction. The samples were investigated for the damping properties using ferromagnetic resonance (FMR) in the frequency range of 6 to 17 GHz. Fig.1 shows the graph between line width (ΔH) and frequency for $t_{\text{Pt}} = 3, 5, 10$ nm, which was extracted by FMR absorption peaks. The ΔH was fitted using Kittel

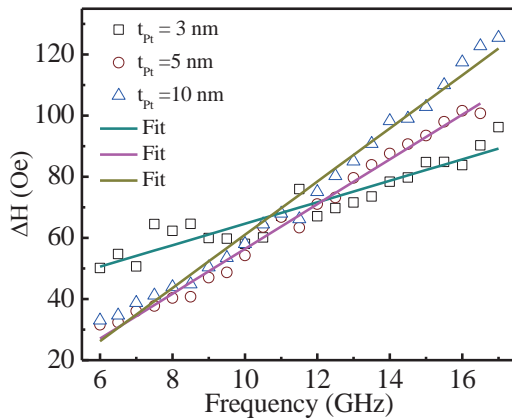


Fig. 1 Frequency dependent line width graph (ΔH) for the sample $t_{\text{Pt}} = 3$ nm (rectangle), 5 nm (circle), 10 nm (triangle). Solid lines are fit with Kittel formula for evaluation of α .

formula [2] for extracting the damping coefficient (α). The values of α were obtained to be 0.0053, 0.0109, 0.0131 for $t_{\text{Pt}} = 3, 5, 10$ nm, respectively. It is clear from the values of the α that the thickness of Pt is very important, which is affecting the interfaces and hence dissipation of angular momentum. This enhancement of the α may be due to spin pumping. To confirm this, we performed ISHE measurements at the frequency of 7.0 GHz. Fig. 2 shows the FMR and ISHE measurements. To quantify the spin pumping contribution, we fitted the measured ISHE voltage using Lorentzian function with taking into account the symmetric and anti-symmetric parts of linewidth:

$$V_{\text{meas}} = V_{\text{sym}} \frac{(\Delta H)^2}{(H-H_{\text{res}})^2 + (\Delta H)^2} + V_{\text{Asym}} \frac{2\Delta H(H-H_{\text{res}})}{(H-H_{\text{res}})^2 + (\Delta H)^2},$$

(1)

where H_{res} is the resonance magnetic field. The values of symmetric component and anti-symmetric component are evaluated as $V_{\text{sym}} = -1.01037 \mu\text{V}$ and $V_{\text{Asym}} = -0.574601 \mu\text{V}$, respectively. Therefore, it can be concluded

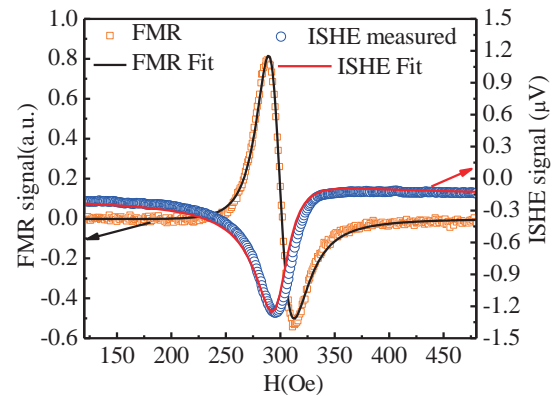


Fig. 2 ISHE voltage and FMR signal versus applied field (open symbol). The red solid line is the fit using Lorentzian function (1).

that the spin pumping is the dominating in our bilayer samples. However, angle dependent ISHE measurements are required for excluding other galvanometric effects like anomalous Hall effect or anisotropic magnetoresistance. These measurements are in progress.

References

- [1] J. Sinova, S. O. Valenzuela, J. Wunderlich, C. H. Back, and T. Jungwirth, *Rev. Mod. Phys.* 87, 1213 (2015).
- [2] C. Kittel, *Phys. Rev.* 73, 155 (1948).

Keywords: Half metal, ferromagnetic, thin films

Full Name: Dr. Subhankar Bedanta, NISER-Bhubaneswar, India-752050,

E-mail: sbedanta@niser.ac.in

Observation of pressure effect on excitation spectra in the triangular-lattice antiferromagnet Cs_2CuCl_4

The effect of pressure on the spin dynamics in Cs_2CuCl_4 , a spin-1/2 Heisenberg antiferromagnet on a triangular lattice, was studied by means of high-field electron spin resonance spectroscopy. A pronounced shift of the exchange mode under applied pressure was observed in the fully spin-polarized phase. Our finding clearly suggests that pressure can be used as a tuning parameter, controlling spin-Hamiltonian parameters in Cs_2CuCl_4 .

Spin-1/2 Heisenberg antiferromagnets on triangular lattices form an important class of low-dimensional spin systems, allowing to probe effects of quantum fluctuations, magnetic order, and frustrations. Among other frustrated spin systems, Cs_2CuCl_4 and Cs_2CuBr_4 are two the most prominent members of the this family. Although magnetic properties of these two materials are very well studied, a lot of important questions still remain open. One of the main problem to solve is the presence of 1/3 and 2/3 saturation magnetization plateaus, which were revealed in Cs_2CuBr_4 , but not the in isostructural material Cs_2CuCl_4 [1]. The reason of such striking difference (and some other very important peculiarities) remains unclear. Systematic electron spin resonance measurements of Cs_2CuCl_4 and Cs_2CuBr_4 have been performed by us. Studying the magnetic excitations spectrum in the magnetically saturated phase allowed us to accurately describe the magnetic excitation spectra in both materials and, using the harmonic spin-wave theory, to determine their exchange parameters [2]. Apart from that, in Cs_2CuBr_4 we observed the presence of a substantial zero-field energy gap, ~ 10 K. The experimental data are compared with results of model spin-wave-theory calculations for spin-1/2 triangle-lattice antiferromagnet, revealing very good agreement [3].

In the present research, the pressure is served as a tuning parameter, a critical behavior between 1D and 2D spin dynamics can be expected. Such experiment will allow us to obtain better understanding of effects of geometrical frustration in these materials, and to study the pressure-tuned quantum critical properties of these and related materials. It is also important to mention that this kind of tunable-frequency high-field and high-pressure ESR experiments is unique, and have never been performed

before. We are very much confident that our high-field and high-pressure ESR measurements will stimulate further interest of the high-field research community worldwide to use this unique facilities at IMR.

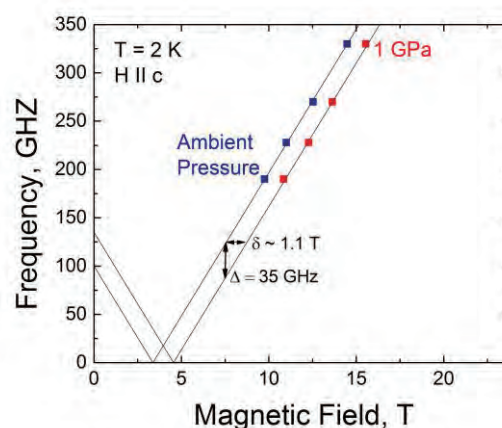


Fig.1 The frequency-field diagram of magnetic excitations in Cs_2CuCl_4 with magnetic field, applied along the c-axis at ambient pressure (blue symbols) and 1 GPa (red symbols).

The effect of pressure was observed in Cs_2CuCl_4 for magnetic field applied above the saturation field ($H_{\text{sat}} = 8$ T) along the c-axis. We found that the application of a pressure of 1 GPa shifts the resonance field of exchange mode (whose position is determined mainly by the zigzag interchain coupling, J' [2]) by more than 1 T (see Fig. 1). In the 2018, we continued the investigation and obtained the systematic high-field ESR data up to 2 GPa. We found a considerable change of exchange parameters leading to the pressure induced quantum phase transition.

References

- [1] T. Ono *et al.*, *Theor. Phys. Suppl.* **159**, 217 (2005).
- [2] S.A. Zvyagin *et al.*, *Phys. Rev. Lett.* **112**, 077206 (2014).
- [3] S.A. Zvyagin *et al.*, *New J. Phys.* **17**, 113059 (2014).

Keywords: high magnetic field, high Pressure, Quantum Phase Transition

S. Zvyagin (Helmholtz-Zentrum Dresden-Rossendorf)

E-mail: s.zvyagin@hzdr.de

<https://www.hzdr.de/db/Cms?pOid=14334&pNid=428>

Comprehensive study of transparent ceramic and single crystal for scintillator

Hafnium based transparent ceramics for scintillation materials were fabricated with Spark Plasma Sintering (SPS) method. $\text{La}_2\text{Hf}_2\text{O}_7$ doped with Tb had green emission under alpha ray and gamma ray excitation, and these materials can be used for current-mode scintillation materials with high detection efficiency.

Scintillators are required in various fields such as medical imaging or astronomy, and high gamma-ray stopping power is required; cross-section of the photo-absorption σ is proportional to Z_{eff}^a , where $a = 4-5$ and Z_{eff} is effective atomic number. $\text{Lu}_2\text{SiO}_5:\text{Ce}$ (LSO), $(\text{Lu},\text{Y})_2\text{SiO}_5:\text{Ce}$ (LYSO) or $\text{Lu}_3\text{Al}_5\text{O}_{12}$ scintillators are used in medical imaging or other applications, because Lu has a high atomic number of 71 and the materials have high stopping power. On the other hand, such a crystal has intrinsic background due to ^{176}Lu decay, and the resulting noise worsens the gamma-ray detection sensitivity.

Hafnium has a high atomic number of 72, and total abundance of its radio isotopes is less than 0.2% (^{174}Hf , half-life is more than 10^{15} year). Thus, a new scintillator consisting of Hafnium can have low intrinsic background and high detection efficiency, thus an efficient scintillator can be developed. However, hafnium itself and hafnium compounds have generally high melting temperatures of more than 2,300 °C. Due to the high melting- temperature, it is difficult to grow the crystal from the melt using conventional crystal growth methods such as Czochralski, Bridgman, and micro-pulling down method [1].

This time, we have fabricated RE-doped $\text{La}_2\text{Hf}_2\text{O}_7$ (LHO), where RE=Tb, Eu. $\text{La}_2\text{Hf}_2\text{O}_7$ has Pyrochlore superstructure. Figure 1 shows the Tb:LHO ceramics sample and its emission spectrum excited by alpha rays. Moreover, Eu-doped LHO had red emission. These emissions were originating from Tb^{3+} or Eu^{3+} 4f-4f transitions, whose decay times were over 10 μsec . Thus, we can use these scintillation materials in current mode detection, not single photon counting method.

We succeeded in preparation of green emission scintillator with high effective atomic number of around 61-62. Here, a Si-avalanche photodiode (Si-APD) has high quantum efficiency than conventional photo-multiplier tube, and the Si-APD has maximum quantum efficiency around the green region.

Thus, these materials can be used for some radiation dose monitor with current-mode using Si-APD or other Si-based detectors.

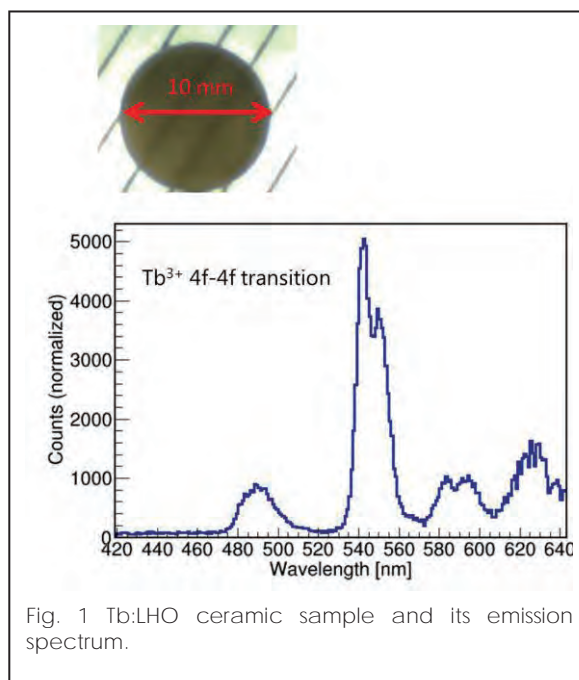


Fig. 1 Tb:LHO ceramic sample and its emission spectrum.

References

- [1] A. Yoshikawa, T. Satonaga, K. Kamada, H. Sato, M. Niki, N. Solovieva, T. Fukuda, J. Cryst. Growth 270 (2004) 427-432

Keywords: optical oxide ceramic

Akira Yoshikawa (Advanced Crystal Engineering) , Georges Boulon (Université Claude Bernard LYON1)

E-mail: yoshikawa@imr.tohoku.ac.jp, georges.boulon@univ-lyon1.fr

<http://yoshikawa-lab.imr.tohoku.ac.jp/>

High-Frequency/Field Electron Paramagnetic Resonance and High-Field Magnetization Studies on Wheel-like Clusters

Abstract: A family of 3d-4f wheel-like clusters $\{\text{Fe}_8\text{Ln}_8\}$ ($\text{Ln} = \text{Gd}, \text{Tb}, \text{Dy}, \text{Ho}, \text{Er}$) and a giant 4f wheel-like cluster $\{\text{Dy}_{20}\}$ were isolated and studied by high-frequency/field electron paramagnetic resonance (HF-EPR) and high-field magnetization. HF-EPR spectra are observed in $\{\text{Fe}_8\text{Ln}_8\}$, which can help to exact the magnetic exchange-coupling constants, while magnetic hysteresis loops were observed for $\{\text{Dy}_{20}\}$, indicating a wheel-like single-molecule magnet.

Wheel-like clusters sometimes display fantastic magnetic properties because of their non-collinear arrangement of their spins. For example, the giant hetero-spin ring $\{\text{Cr}_8\text{Dy}_8\}$ is a single-molecule magnet with open magnetic hysteresis loop at 0.5 K [1]. Toroidal behavior were observed in $\{\text{CrTb}_6\}$ and $\{\text{CrHo}_6\}$ molecules at low temperatures [2], and $\{\text{CrDy}_6\}$ analogy displays a ferrotoroidic ground state [3]. Such behaviors are probably arising from magnetic coupling with strong single-ion anisotropy. Understanding of the exchange coupling in wheel-like clusters is of great importance to design complexes with toroidal moments and molecule-based multiferroics.

Herein, A series of hexadenuclear heterometallic wheel-like molecular clusters $\{\text{Fe}_8\text{Ln}_8\}$ ($\text{Ln} = \text{Gd}, \text{Tb}, \text{Dy}, \text{Ho}, \text{Er}, \text{Y}$) and a family of giant lanthanide $\{\text{Dy}_{20}\}$ were isolated. Their structures were studied by single crystal X-ray diffraction, revealing similar giant ring structure for all complexes. High-frequency/field electron paramagnetic resonance (HF-EPR) and high-field magnetization measurements were carried out for those complexes at low temperature to investigate the exchange coupling in those wheel-like clusters.

Fig.1 shows HF-EPR spectra at 4.2 K for $\{\text{Fe}_8\text{Gd}_8\}$ (1a), $\{\text{Fe}_8\text{Tb}_8\}$ (1b), $\{\text{Fe}_8\text{Dy}_8\}$ (1c), $\{\text{Fe}_8\text{Ho}_8\}$ (1d), and $\{\text{Fe}_8\text{Er}_8\}$ (1e) with crystal structure for $\{\text{Fe}_8\text{Ln}_8\}$ (1f). From the crystal structure, the Fe(III) ions and Ln(III) ions are arranged alternately to form a ring. The Fe...Ln separations are in the range from 3.39 to 3.48 Å. To get the exchange couplings in those clusters, both magnetic and HF-EPR measurements were carried out. In the $\{\text{Fe}_8\text{Gd}_8\}$ system, ferromagnetic interactions between Fe-Gd metal centers were found to be dominant from the magnetic susceptibilities, while with HF-EPR studies, the

level-crossing field (H_c), together with the g factor and energy gap (ΔE) can be determined from extrapolation in these plots (Figure 1 and table 1). Combined with the magnetic susceptibilities, we are going to determine the exchange couplings between Fe(III) ions and Ln(III) ions with the method reported by Prof. Hiroyuki Nojiri et al. [4-5].

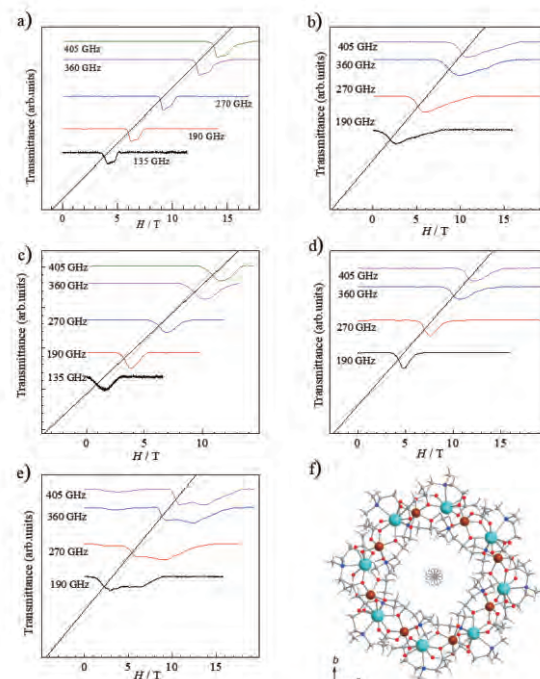


Fig. 1 Selected HF-EPR spectra of $[\text{Fe}_8\text{Ln}_8]$ measured at 4.2 K [$\text{Ln} =$ (a) Gd, (b) Tb, (c) Dy, (d) Ho and (e) Er]. The spectra are offset in a linear scale of the frequency. Straight line are drawn from the linear fitting in the frequency field plot. (f) Ball-and-stick modes of the molecular structures of $\{\text{Fe}_8\text{Ln}_8\}$ wheels.

Table 1 The level-crossing fields (H_c) and energy gap (ΔE) from linear fitting in the frequency field plot for $\{\text{Fe}_8\text{Ln}_8\}$ wheels.

	Fe_8Gd_8	Fe_8Tb_8	Fe_8Dy_8	Fe_8Ho_8	Fe_8Er_8
H_c / T	-0.60	-4.35	-3.30	-2.18	-4.02
$\Delta E/\text{GHz}$	16.45	111.72	88.32	58.45	105.35

The structure of another wheel-like cluster $\{Dy_{20}\}$ was shown in the Fig 2a, which is consisting of 20 Dy(III) ions bridged by 20 piv and 30 2-pa ligands with central water molecules and inner pyridine rings as template and terminal OH⁻ groups to balance the positive charge. At 0.45 K, magnetic hysteresis loops can be clearly observed (Fig 2b), which is indicative of a single-molecule magnet. Such behavior is in good agreement with its temperature dependent ac susceptibility data above 2 K, in which tail of out-of-phase signals can be observed. The energy barrier is probably very low with strong quantum tunnelling of the magnetization.

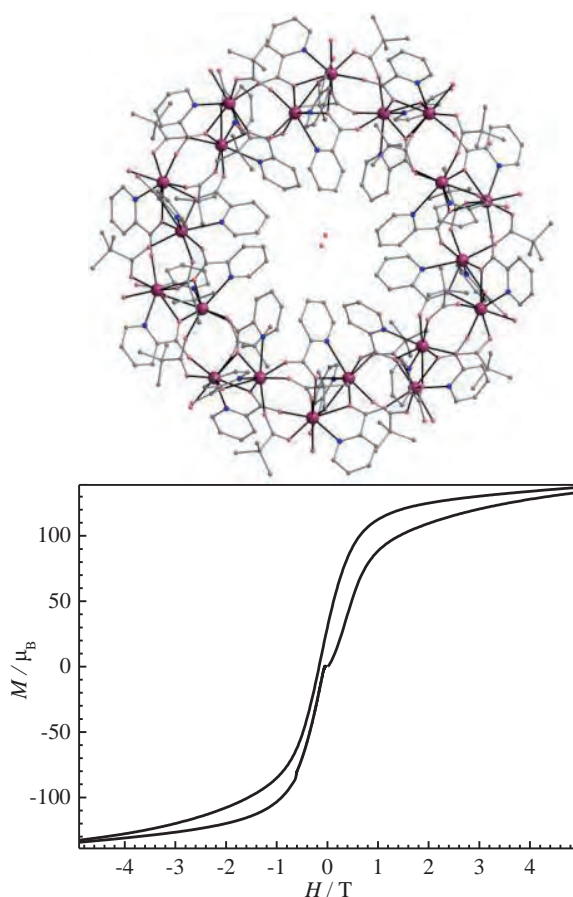


Fig. 2 (a) Molecular structure of $\{Dy_{20}\}$. Color code: Ln, purple; O, pink; N, blue; C, grey. (b) Magnetic hysteresis loop at 0.45 K for $\{Dy_{20}\}$

also carried out for a three-coordinated Fe(III) momer $\{Fe(NTMS_2)_3\}$, a two-coordinated Cr(II) momer $\{Cr(SDipp)_2\}$ and a giant 3d-4f cluster $\{Ni_{36}Ln_{96}\}$. High-field magnetization measurements were carried for wheel-like molecular clusters $\{Fe_8Ln_8\}$ (Ln = Gd, Tb, Dy, Ho, Er, Y). Analysis of those data were undergoing and we believed we believe we can get a lot of useful information from those data.

In conclusion, we got some HF-EPR spectra and high-field magnetizations for two kinds of wheel-like clusters. With magnetic susceptibilities and theoretical studies, we will have a clear understanding about electronic structure in those wheel-like clusters. With better and clearer understanding of the magneto-structural correlation, electronic structure and energy levels of those wheel-like clusters, single-molecule toroidal behavior may be clarified. We wish to publish three research papers in high-profile journals using these results.

We would like to acknowledge the financial support from Institute for Materials Research and High Field Laboratory. Prof. Hiroyuki Nojiri are gratefully acknowledged for all the technical support, measurements and analysis of the data. We are also is thankful to Miss Nanae Tadano assist with all object for this trip.

References

- [1] L. Qin, J. Singleton, W. P. Chen, H. Nojiri, L. Engelhardt, R. E. P. Winpenny and Y. Z. Zheng, *Angew. Chem. Int. Edit.*, 2017, **56**, 16571-16574.
- [2] K. R. Vignesh, S. K. Langley, A. Swain, B. Moubaraki, M. Damjanovic, W. Wernsdorfer, G. Rajaraman and K. S. Murray, *Angew. Chem. Int. Edit.*, 2018, **57**, 779-784.
- [3] K. R. Vignesh, A. Soncini, S. K. Langley, W. Wernsdorfer, K. S. Murray and G. Rajaraman, *Nat. Commun.*, 2017, **8**: 1023.
- [4] R. Watanabe, K. Fujiwara, A. Okazawa, G. Tanaka, S. Yoshii, H. Nojiri and T. Ishida, *Chem. Commun.*, 2011, **47**, 2110-2112.
- [5] T. Shimada, A. Okazawa, N. Kojima, S. Yoshii, H. Nojiri and T. Ishida, *Inorg. Chem.*, 2011, **50**, 10555-10557.

Keywords: magnetic properties, high magnetic field, electron spin resonance
 You-Song Ding, Frontier Institute of Science and Technology, Xi'an Jiaotong University
 High Field Laboratory for Superconducting Material
 E-mail: nojiri@imr.tohoku.ac.jp
[http:// www.hfpm.imr.tohoku.ac.jp/](http://www.hfpm.imr.tohoku.ac.jp/)

Synchronized Magnetic Field and X-ray Pulses to Study Quantum Matter in Extreme Conditions

X-ray scattering technique is a powerful tool to study symmetry breaking phenomena in quantum materials. The recent development of brilliant x-ray free-electron laser (FEL) sources is now pushing the limit of photonic scattering techniques to new levels. Here, we aim at exploring uncharted territory of quantum matter physics by the synchronization of x-ray FEL pulses and magnetic field pulses under extreme sample environment.

The experimental platform for single-shot x-ray scattering experiment is being developed at SwissFEL free-electron laser through a collaboration of Tohoku University (Prof. Nojiri), University of Zurich (Prof. Chang) and Paul Scherrer Institut (Dr. Gerber). The intense femtosecond x-ray pulses from the SwissFEL will be synchronized with millisecond high magnetic field pulses of up to 35 Tesla at a minimum temperature below 2 Kelvin. The scientific potential of this scheme was demonstrated at the LCLS x-ray FEL in 2015, where Prof. Nojiri and Dr. Gerber were key actors [1, 2].

Two young researchers, Dr. Choi (postdoc) and Rechsteiner (scientific engineer), visited Prof. Nojiri's group through the ICC-IMR single visit program. We had technical discussions and achieved considerable progress in the collaboration project.

First of all, we finalized a prototype design of dual-cryostat experimental platform (Fig. 1). Fruitful feedbacks and advices were provided by Prof. Nojiri's team, based on rich experience in similar developments. We gained knowledge in designing kapton windows, magnet holders/leads, and cryogenic wiring (Fig. 2). The transferred knowledge is being essentially used for realization of our experimental setup.

To reach temperature below 2 Kelvin, minimization of thermal loss is of utmost importance. We discussed how to improve thermal contact and cooling efficiency of both sample and pulsed magnet assembly, based on finite-element method (FEM) heat transfer modeling. As a result, we reached a conclusion that installation of radiation shields enables us to achieve a minimum sample temperature below 2 Kelvin. Proper design of heat sinks and cold fingers is also important to reduce temperature on magnet assembly and its duty cycle. The thermal conductivity of magnet assembly might be improved by use of sapphire core.

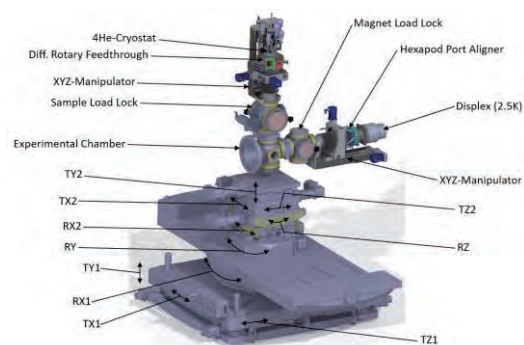


Fig. 1. Dual-cryostat platform containing pulsed magnet coils for the x-ray scattering experiment at SwissFEL

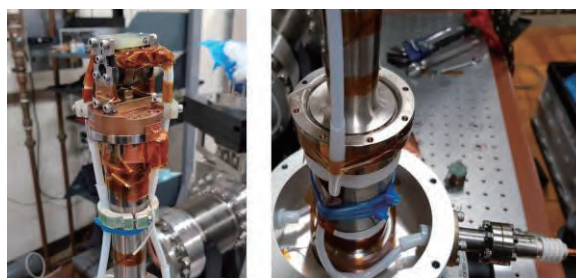


Fig. 2. (Left) Photo of pulsed magnet assembly mounted on a pulse-tube-type cryostat. (Right) Photo of magnet leads and feedthroughs. Both photos were taken at Prof. Nojiri's research group.

To sum up, the IMR-ICC single visit program was an excellent starting point in establishing a long-term collaboration between IMR, PSI and UZH for the single-shot x-ray scattering experiment at SwissFEL under pulsed magnetic field. Time and work plan for future cooperation to test the instrument and to conduct experiment is being organized for achieving successful collaboration.

References

- [1] S. Gerber *et al.*, *Science* **350**, 949 (2015).
- [2] H. Jang *et al.*, *Proc. Natl. Acad. Sci. USA* **113**, 14645 (2017).

Keywords: x-ray diffraction (XRD), high magnetic field, superconducting
 Jaewon Choi and Dominik Rechsteiner (Physik-institut, University of Zurich)
 E-mail: jchoi@physik.uzh.ch
<http://www.physik.uzh.ch/groups/chang/index.php>

Activity Report

Young Researcher Fellowships



FY 2017 Young Researcher Fellowships

No.	Name	Host	Proposed Research	Title	Affiliation	Term
17FS01	Karol Andrzej Bartosiewicz	Prof. Yoshikaka	Growth and Study of Multicomponent Garnet Scintillators	Post Doctor	Institute of Physics, Academy of Sciences of the Czech Republic	2017.4.19-7.17
17FS02	Zhao Tianqi	Prof. Bauer	First Principles Approach to Spin Relaxation Time in Anisotropic Semiconductor	PhD Student	Tsinghua University, China	2017.7.29-12.4
17FS03	Jonathan Hughes	Prof. Nagai	Early Stage Precipitate Formation in Cu-based Alloys for Nuclear Fusion Reactors	PhD Researcher	University of Manchester, UK	2017.7.17—9.2
17FS04	Chalernpol Rudradawong	Prof. Goto	Fabrication of $12\text{CaO}\cdot 7\text{Al}_2\text{O}_3$ Cement by Spark Plasma Sintering for Thermoelectric Applications	PhD Student	King Mongkut's Institute of Technology Ladkrabang, Thailand	2017.11.5-2018.1.12

Growth and study of multicomponent garnet scintillators

Aluminum garnets, $(Y,Lu)_3Al_5O_{12}:Ce$ are a promising candidate for the next generation of the efficient scintillators [1]. However, they suffer from the contribution of the undesired slow component in the scintillation response [2]. The Mg^{2+} codoping strategy might improved some scintillation characteristic.

During my stay in Professor Yoshikawa Laboratory at the Institute for Materials Research, Tohoku University I received accurate training in the growing of single crystals of oxides from the melt. My training was focused on the micro-pulling-down method. Using this technology, I successfully grew mixed garnet scintillation fibers. Totally I grew 2 series (10 single crystals) of Ce-doped and Mg-codoped LuYAG single crystals with various Lu/Y ratio to test the influence of Y admixture and Mg-codoping on the scintillation response. The Mg content in the grown crystals was 200 and 400 ppm, whilst the concentration of Ce was 200 ppm in all grew samples. Figure 1 shows the example of the grown $Y_{0.25}Lu_{0.75}Al_5O_{12}:Ce,Mg$ single crystal (length ~4 cm, diameter ~2.5 cm). The Mg^{2+} codoping creates an additional fast radiative recombination pathway, which can efficiently compete in electron trapping from the conduction band with the shallow electron traps in the YAG and LuAG host lattice [3]. Such a pathway is realized by the stabilization of a tetravalent Ce^{4+} center in the garnet lattice by divalent rare earth ion co-doping.

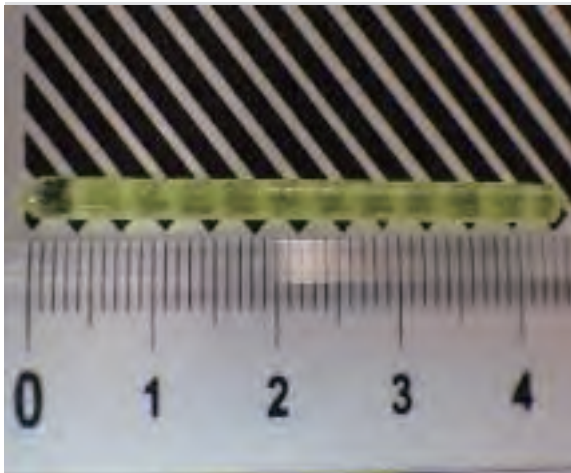


Fig. 1. Picture of $Y_{0.25}Lu_{0.75}Al_5O_{12}:Ce,Mg$ single crystal

The presence of the stable Ce^{4+} luminescence centers in the grown crystals is clearly visible on the Fig. 2 by fingerprinted charge transfer absorption transition of the Ce^{4+} starting from 360 nm [4].

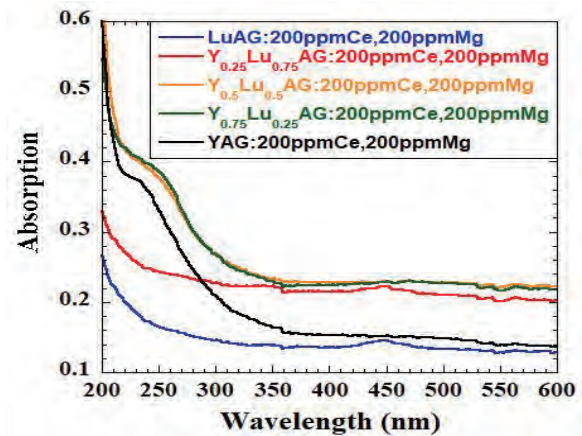


Fig. 2 The RT absorption spectra of $(Y,Lu)_3Al_5O_{12}:Ce$ single crystals

Moreover, the $4f \rightarrow 5d_2$ and $4f \rightarrow 5d_1$ absorption transitions of the stable Ce^{3+} are not detected on the absorption spectra. This observation might suggest that relatively high content of Mg^{2+} ions transforms almost all stable Ce^{3+} luminescence centers into stable Ce^{4+} , which was the aim of this study. The high content of the of the stable Ce^{4+} luminescence centers in the grown single crystals might have positive impact on the scintillation characteristics. Namely, can significantly increase scintillation response and eliminate undesired rise time. However, at the same time it can reduce scintillation light yield value. More detailed measurements of the grown crystals will be performed at the group of Professor Marin Nikl at the Institute of Physics of the Czech Academy of Sciences in Prague, Czech Republic.

References

- [1] M. Nikl, A. Yoshikawa, Adv. Optical Mater. 3, 463-481 (2015).
- [2] M. Lucchini et al., Instr. Meth. Phys, Research A 852, 1-9 (2017).
- [3] M. Nikl, et al., Growth Des. 14, 4827 (2014).
- [4] Y. Wu, et al., Phys. Rev. Applied 2, 044009 (2014),

Young Researcher Fellowships

Keywords: crystal growth, luminescence, optical absorption

Full Name (Division Name or Affiliation) Karol Andrzej Bartosiewicz, Institute of Physics, Academy of Sciences of the Czech Republic

E-mail: karol@imr.tohoku.ac.jp

Elliot-Yafet Spin Relaxation Time for Elemental Two-dimensional Materials from First-Principles Calculations

We have studied the Elliot-Yafet spin relaxation time for elemental two-dimensional materials, including graphene, silicene, germanene, stanene, arsenene and antimonene. The Elliot-Yafet spin relaxation time is correlated to momentum relaxation time by the spin mixing parameter $\langle b^2 \rangle$. Large anisotropy for Elliot-Yafet spin relaxation time was revealed for these two-dimensional materials between in-plane and out-of-plane directions.

Long spin relaxation times are obviously advantageous for most applications of spintronics. In recent years, the spin relaxation time for two-dimensional materials has attracted the attention from both experimental [1] and theoretical [2] groups. In the commonly used non-local measurements, ferromagnetic metal electrodes inject and detect spins in normal conductors. Spin relaxation in a non-magnetic conductor is the physical process that restores a non-equilibrium spin polarization to the un-polarized equilibrium state. Two spin relaxation mechanisms are considered in normal metals and doped semiconductors: 1) the Elliot-Yafet mechanism, which is caused by ordinary scattering by phonons, impurities, boundaries or interfaces; 2) the D'yakonov-Perel' mechanism, which is important in systems with broken inversion symmetry that generate momentum-dependent internal magnetic fields and cause spin precession.

All elemental two-dimensional materials are inversion symmetric, which means that the D'yakonov-Perel' mechanism is extrinsic, i.e. active only in the presence of external fields or

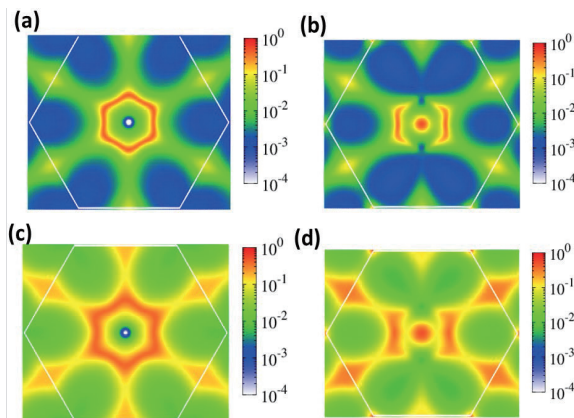


Fig. 1 Spin-mixing parameter b_k^2 over the first Brillouin zone of arsenene for holes in (a) the out-of-plane direction and (b) in-plane armchair direction. (c) and (d) same as (a) and (b), respectively, but for antimonene.

due to the interaction with substrates Here we focus on the Elliot-Yafet spin relaxation time, which can be computed by the simplified relation

$$1/\tau_{s,EY} \approx 4 \langle b_{nk}^2 \rangle / \tau_k,$$

where τ_k is the momentum relaxation time caused by phonon scattering (for which we assume the typical value of 100 fs). $\langle b_{nk}^2 \rangle$ is the Fermi-Dirac distribution averaged spin-mixing parameter that accounts for the effects of spin-orbit coupling on the electronic eigenstates (which also causes the deviations of the g -factor from 2 for electrons in solids).

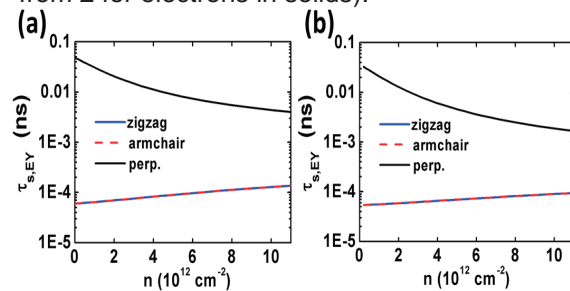


Fig. 2 Elliot-Yafet spin relaxation time as a function of hole density at 300 K in (a) arsenene and (b) antimonene for in-plane (zigzag and armchair) and out-of-plane directions (perp.).

Figs. 1 and 2 show the spin-mixing parameter and spin relaxation time for arsenene and antimonene, respectively. We reveal a large anisotropy between in-plane and out-of-plane directions for the Elliot-Yafet spin relaxation time with $\tau_{\parallel}/\tau_{\perp} \approx 0$ also for the other two-dimensional materials

We plan to also calculate spin relaxation by the D'yakonov-Perel' mechanism in order to be in a position to compare theory with experiments.

References

- [1] W. Han, R. K. Kawakami, M. Gmitra and J. Fabian, Nat. Nanotechnol. **9**, 794-807 (2014).
- [2] M. Kurpas, M. Gmitra, and J. Fabian, Phys. Rev. B. **94**, 155423 (2016).

Keywords: spintronic, first principles calculations, elemental
Tianqi Zhao (Chemistry Department, Tsinghua University, Beijing, China)
E-mail: zhaotq13@mails.tsinghua.edu.cn
<http://www.shuagroup.net>

Early Stage Precipitate Formation in Cu-based Alloys for Nuclear Fusion Reactors

Abstract: This report details the progress of a research project into the ageing behaviour of CuCrZr alloys, carried out at IMR-Oarai and continued at the University of Manchester. In the initial stage of the ageing, the hardness and positron lifetime showed the similar ageing trends, suggesting that vacancy-type defects contribute to the hardening. The defects may be associated with Zr atoms.

Cu_{1.0}Cr_{0.1}Zr Alloys are the alloy of choice for use as a heat exchange component in the ITER fusion reactor thanks to their high conductivity combined with their superior mechanical strength induced through precipitation hardening [1]. The mechanisms taking place during the ageing process are not well understood, in particular the role that Zr plays in precipitate formation. To investigate this, PAS and microhardness testing was carried out on CuCrZr and CuCr samples, aged for a range of times up to 4 hours, and comparisons between the two were made.

The PAS results obtained during the time in Oarai showed that CuCrZr alloys had a similar vacancy no. density to CuCr but the vacancies were slightly larger in CuCrZr (V₄ as opposed to V₂), however no pattern emerged with regards to aging time. (Fig 1a & 1b) Microhardness testing results (Fig. 1a) indicate why this is the case, showing microhardness testing results on CuCrZr and CuCr alloy samples tested in Oarai, as well as new samples created after returning to Manchester.

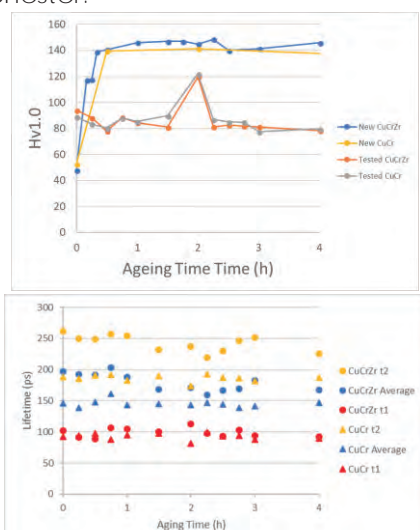


Fig 1: a.) Microhardness results for all samples
b.) Positron lifetime results for all samples

As one can see in Fig. 1, the PAS tested samples show little change across the first 4 hours of ageing, as indicated in the closely correlated positron lifetime and microhardness results. However, this was not expected, so new samples were created after returning to Manchester, indicating the tested samples had been oxidized during the heat treatment process.

In Fig. 1a, hardness results for the new samples revealed that ageing creates a rapid increase in hardness up to around 30 minutes before levelling off. Because of this, the new set of samples to be PAS tested will focus on the first 30 minutes of ageing. PAS results do suggest a link between Zr and the defects in CuCrZr (Fig. 2).

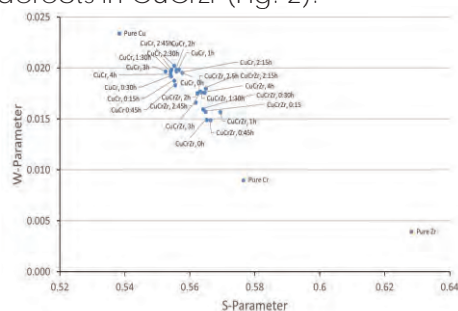


Fig 2: S vs. W parameter for tested samples
Plotting S vs. W parameter shows that the 0.1% Zr has the effect of increasing the proportion of low momentum annihilations (S-parameter), indicating that Zr plays a role in the formation of larger defects in CuCrZr as opposed to CuCr. In order to complete the experiment and characterize the association between Zr and the larger defects present in CuCrZr, PAS testing of a new set of CuCrZr and CuCr samples is still ongoing, with APT work to take place to support these results.

References

[1] S.J. Zinkle, "Applicability of copper alloys for DEMO high heat flux components", Phys. Scr., vol. T167, no. T167, p.14004, 2016

Keywords: Positron annihilation, microstructure
Full Name Jonathan Hughes (University of Manchester)
E-mail: jonathan.hughes-7@postgrad.manchester.ac.uk

Fabrication of $\text{Ca}_{12}\text{Al}_{14}\text{O}_{33}$ mayenite structure by spark plasma sintering

In this work, the $\text{Ca}_{12}\text{Al}_{14}\text{O}_{33}$ (C12A7) compounds were consolidated by spark plasma sintering (SPS) at 1100, 1200, 1300 and 1350 °C for 5 min, 50 MPa. The XRD result indicated the C12A7 phase in all specimens. The relative density increased from 87.1 to 99.4% with increasing sintering temperature. The electrical conductivity was also enhanced by increasing sintering temperature. The C12A7 specimens sintered at 1350 °C showed the highest electrical conductivity of 1.96 S m^{-1} at 800 °C.

C12A7 compounds are a promising candidate for functional applications such as electrode [1], catalyst [2] and thermoelectric materials [3]. The unique structure consists of 12 nano-cages in a cubic unit cell while only 2 cages contain extra O^{2-} ion inside the cage. With the reduction process, the electron can be substituted for the O^{2-} ion, as a result, the carrier concentration for conduction could increase.

The aim of this study is to fabricate C12A7 by SPS under a reduction atmosphere. The SPS method possesses a fast heating rate with an applied pressure which could result in a high density product. The vacuum and the diffusion of carbon from graphite mold might induce the reduction atmosphere surrounding specimen. This could be the key factor to improve the electrical properties of C12A7.

Figure 1 shows XRD patterns of the sintered specimens and calcined powder. All sintered specimens were indicated as C12A7 (JCPDS no. 19-0629). The phase of C12A7 remained stable as increased temperature from 1100 to 1350 °C. However, after increase temperature to 1400 °C, the specimen was melted away.

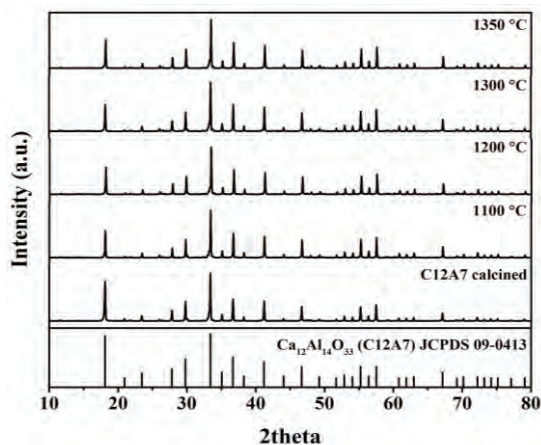


Fig. 1. XRD patterns of C12A7 at various sintering temperature by SPS.

Keywords: C12A7, mayenite, spark plasma sintering

Full Name: Chalermopol Rudradawong, King Mongk't Institute of Technology Lardkrabang, Bangkok, Thailand

E-mail: C.Rudradawong@gmail.com

The relative density of C12A7 increased from 87.1 to 96.6% with increasing temperature from 1100 to 1200 °C. The fully-densified C12A7 with the relative density of 99.4% was obtained at 1300–1350 °C.

Figure 2 shows the temperature dependence of electrical conductivity of C12A7 sintered at various temperature. The electrical conductivity of all specimens increased with the increasing temperature indicating the semiconductor behavior. The C12A7 specimens sintered at 1350 °C showed the highest electrical conductivity of 1.96 S m^{-1} at 800 °C. The improvement in electrical conductivity was possible to be due to two reasons. First, carbon diffused into the structure of C12A7 specimens. Second, carbon reduced the extra O^{2-} in the cage structure.

In conclusion, the high density C12A7 with improving electrical conductivity was achieved by SPS at 1350 °C.

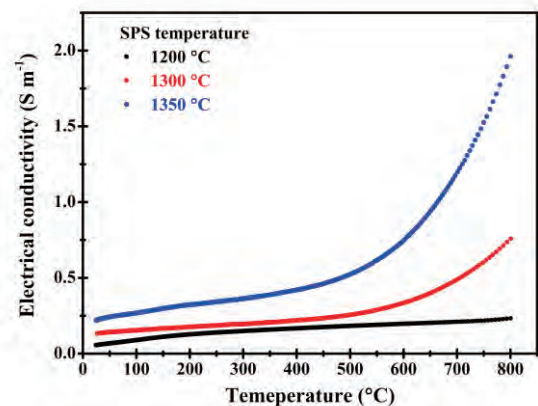


Fig. 2. Temperature dependence of electrical conductivity of C12A7.

References

- [1] Y. Toda et al., *Thin Solid Films*. 445 (2003) 309.
- [2] F. Hayashi et. al, *Chem. Sci.*, 4 (2013) 3124.
- [3] S. W. Kim et. al.. *Phvs. Rev. B.* 80 (2009) 1.

ICC-IMR FY2017 Activity Report

Edited by ICC-IMR Office
Published in August, 2018

Contact: International Collaboration Center,
Institute for Materials Research (ICC-IMR)
Tohoku University
2-1-1, Aoba-ku, Sendai, 980-8577, Japan
TEL&FAX: 81-22-215-2019
E-mail: icc-imr@imr.tohoku.ac.jp

Printing: HOKUTO Corporation

Copyrights © Institute for Materials Research

